

# Analysis and interpretation of the thermal test of gas hydrate dissociation in the JAPEX/JNOC/GSC et al. Mallik 5L-38 gas hydrate production research well

G.J. Moridis<sup>1</sup>, T.S. Collett<sup>2</sup>, S.R. Dallimore<sup>3</sup>, T. Inoue<sup>4</sup>, and T. Mroz<sup>5</sup>

*Moridis, G.J., Collett, T.S., Dallimore, S.R., Inoue, T., and Mroz, T., 2005: Analysis and interpretation of the thermal test of gas hydrate dissociation in the JAPEX/JNOC/GSC et al. Mallik 5L-38 gas hydrate production research well; in Scientific Results from the Mallik 2002 Gas Hydrate Production Research Well Program, Mackenzie Delta, Northwest Territories, Canada, (ed.) S.R. Dallimore and T.S. Collett; Geological Survey of Canada, Bulletin 585, p.*

---

**Abstract:** The objectives of this study were to 1) analyze the data from a field test of thermally induced dissociation of gas hydrate in the JAPEX/JNOC/GSC et al. Mallik 5L-38 gas hydrate production research well; 2) validate and calibrate the numerical model; and 3) determine important parameters describing gas hydrate behaviour and dissociation. The initial conditions and properties of the gas hydrate deposit were determined using supporting geological and geophysical data. Direct measurements provided the necessary boundary conditions. The numerical model was calibrated against the cumulative volumes of produced gas, a process that increased confidence in the model. Two possible scenarios of thermal dissociation, using unadjusted and smoothed data, are proposed to interpret the field test results. The parameters of the dominant physical processes are estimated by inverse modelling (history matching). Their results compare favourably with previously published data. Additionally, estimates of long-term production are made, and an alternative well configuration is proposed to substantially increase gas production.

## Résumé :

---

<sup>1</sup>Lawrence Berkeley National Laboratory, Earth Sciences Division, 1 Cyclotron Road, Berkeley, California, United States 94720

<sup>2</sup>United States Geological Survey, Box 25046, MS-939, Denver, Colorado, United States 80225

<sup>3</sup>Geological Survey of Canada, 9860 West Saanich Road, P.O. Box 6000, Sidney, British Columbia, Canada V8L 4B2

<sup>4</sup>JNOC Technology Research Center, Japan National Oil Corporation, 1-2-2 Hamada, Mihama-ku, Chiba 261-0025, Japan

<sup>5</sup>United States Department of Energy, National Energy Technology Laboratory, 3610 Collins Ferry Road, Morgantown, West Virginia, United States 26507

## INTRODUCTION

### Background

The Mallik gas hydrate field, located at the northeastern edge of Canada's Mackenzie Delta, is situated within a sequence of Tertiary sediments in an area underlain by more than 600 m of permafrost. Detailed geological and engineering data on gas hydrate and associated sediments are available from the original Mallik discovery well, drilled in 1972 (Bily and Dick, 1974), and from a scientific research well program undertaken during the winter of 1998 (Dallimore et al., 1999). Quantitative well-log determinations and core studies reveal at least 10 discrete gas hydrate layers, exceeding 110 m in total thickness, at depths of approximately 900 to 1100 m. The gas hydrate intervals have high gas hydrate saturation values that, in some cases, exceed 80% of the pore volume (Collett et al., 1999; Miyairi et al., 1999). These attributes establish the Mallik field as one of the most concentrated gas hydrate reservoirs in the world. Recognizing that the Mallik gas hydrate accumulation was an ideal site for a field test of gas production from a natural gas hydrate, an international partnership was formed to carry out a production research program in 2002 (Dallimore et al., 2005). A major objective of the program was to observe and analyze the unknown field behaviour of natural gas hydrate during dissociation under controlled conditions, leading to the determination and quantification of the corresponding processes and parameters that affect gas production from gas hydrate.

Field operations for the 2002 Mallik program were carried out during the winter of 2001–2002 (Takahashi et al., 2005). The multidisciplinary field program included completion of JAPEX/JNOC/GSC et al. Mallik 5L-38, an 1188 m deep production well, and Mallik 3L-38 and 4L-38, two observation wells drilled to a similar depth and 40 m distant from the production well. The scientific program included extensive borehole- and surface-geophysical studies, and numerous detailed studies from cores collected through the gas hydrate interval, which was continuously cored from 886 to 1151 m in the Mallik 5L-38 production test well (Dallimore et al., 2005). Gas hydrate production testing included short-duration, small-scale pressure-drawdown tests and a five-day thermal-stimulation test (Satoh et al., 2005).

### Objectives and general approach

The objectives of this study were to

- analyze data from a field test of thermally induced dissociation of gas hydrate in the Mallik 5L-38 research well;
- interpret the data for the identification of plausible scenarios occurring during this dissociation test;
- use the field data for model validation and calibration of the numerical simulator (Moridis, 2003);
- determine important thermal and thermodynamic parameters describing gas hydrate behaviour and dissociation; and
- predict long-term production involving different dissociation methods and alternative production-system configurations.

### Thermal test

The detailed design of the Mallik thermal-production test is discussed in several papers within this publication, including Satoh et al. (2005) and Hancock et al. (2005). The thermal-production test was carried out by circulating hot water across a 13 m perforated gas-hydrate-bearing section from 907 to 920 m. Hot water circulating in the well came in contact with the gas hydrate in the gas-hydrate-bearing formation, causing dissociation of the gas hydrate. Gas from dissociated gas hydrate flowed to the well and was circulated to the surface in the circulating fluid, where it was separated and the produced volume was measured. The pressure was monitored in the wellbore and at the surface, while the evolution of temperatures along the borehole from the surface to below the test interval was continuously monitored by a distributed temperature system (DTS), consisting of a fibre-optic cable strapped on the outside of the production casing (Henninges, 2005).

This study has benefited from a wide range of data (geophysical, geological, hydrological, thermal, operation, and production) available on the geology and gas hydrate properties of the thermal-test interval, collected as part of a broad, multidisciplinary science program over the course of the thermal test (Dallimore et al., 2005). Supporting data include a detailed assessment of the formation geology and boundaries, formation hydraulic properties, pressure, temperature, phase saturations, and initial estimates of the formation wettability properties (relative permeability and capillary pressure functions, and corresponding parameters). Using all the relevant supporting data, as well as operational parameters, the numerical model was validated and calibrated against the cumulative volumes of produced gas through inverse modelling (history matching). The history-matching process yielded estimates of gas hydrate properties and of important dissociation parameters, which were then compared to published-literature data.

## DESCRIPTION OF GEOLOGICAL MODEL AND TEST SYSTEM

### Geology and stratigraphy of the gas hydrate formation

The geology of the Mallik gas hydrate field has been extensively described in numerous publications (*see* Dallimore and Collett, 1999; Jenner et al., 1999; Dallimore et al., 2005). The gas-hydrate-bearing formation targeted in the thermal test extended from 906 to 930 m in depth. As described by Satoh et al. (2005), the thermal-production-test interval was chosen to optimize the effectiveness of the test. An interval was chosen with uniform gas hydrate characteristics and some degree of lithological isolation above and below the zone. The detailed characteristics of the thermal-production interval can be interpreted on the basis of a composite well-log montage presented in Figure 1. Well-log derivations suggest that the production interval from 907 to 920 m has high gas hydrate saturation values, with up to 85% of the pore space being occupied by gas hydrate. Fine-grained silt intervals with low to no gas hydrate content bound the gas hydrate interval above and below. Core studies suggest the sediment

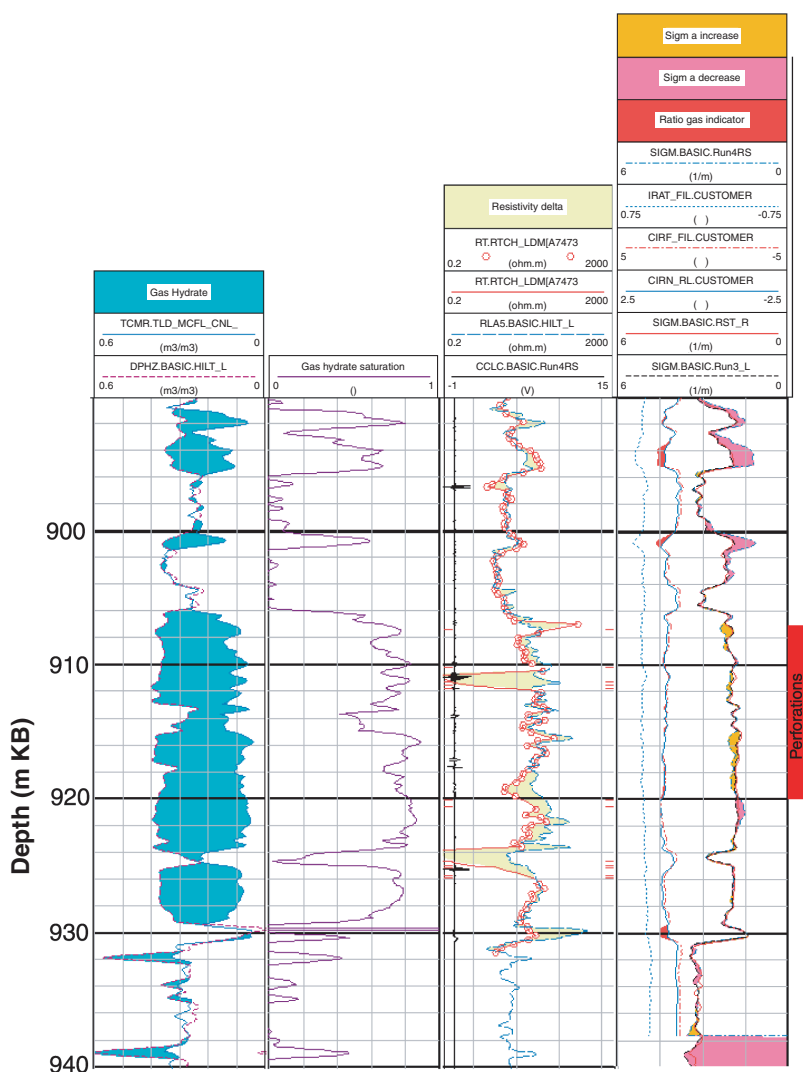
in the production interval is largely coarse-grained sand; however, a 2 m gravel layer was observed at a depth of 913 to 915 m.

Moridis and Collett (2003) have developed a simple classification system for naturally occurring gas hydrate deposits, describing three classes on the basis of gas hydrate and free-gas associations. Class 1 and 2 gas hydrate deposits are characterized by a gas-hydrate-bearing layer underlain, respectively, by a two-phase zone involving mobile gas and a single-phase zone of mobile water. The thermal-test interval in the Mallik 5L-38 well would be a Class 3 deposit, containing only gas hydrate that is not associated with a free-gas or mobile-water zone.

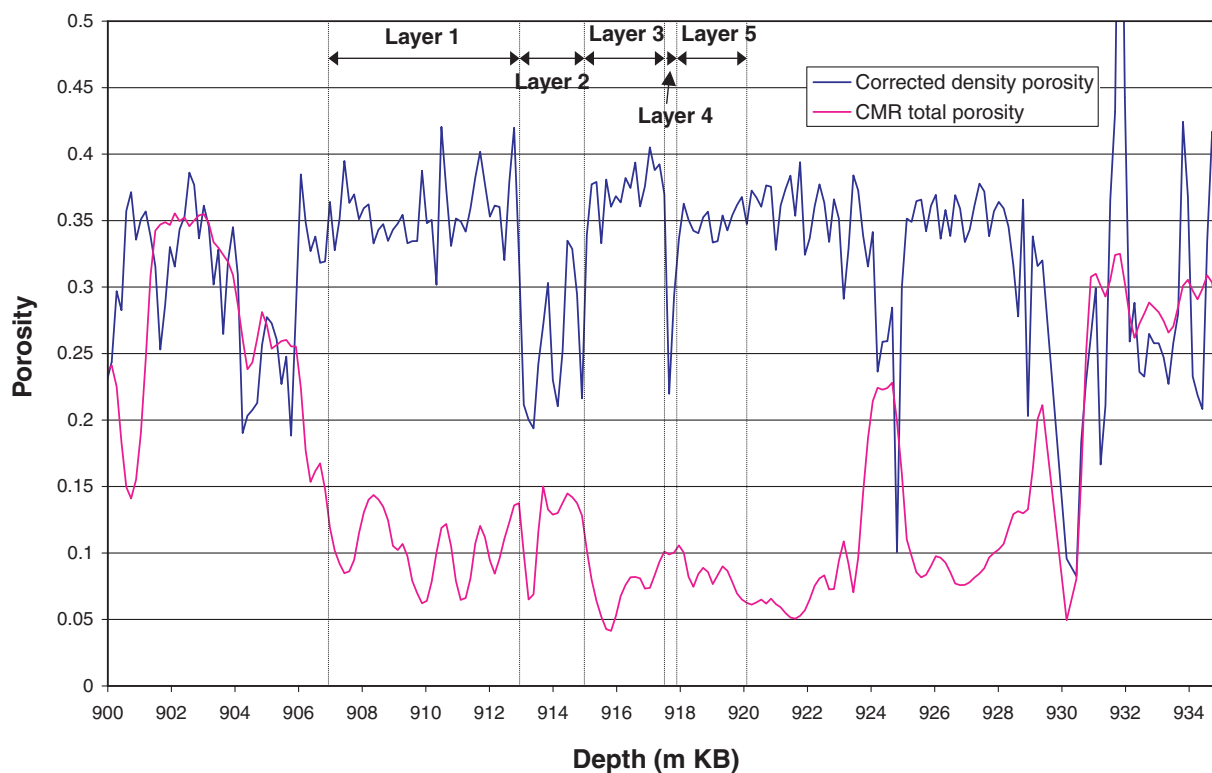
### ***Hydraulic and wettability properties of the gas-hydrate-bearing formation***

Figure 2 shows the porosity distribution in the gas-hydrate-bearing thermal-test interval, as estimated from NMR- and density-log measurements (Lewis and Collett, 2005). The five layers identified in the gas hydrate interval (shown in Fig. 2) have average porosities ( $\phi$ ) of 0.35, 0.25, 0.38, 0.27, and 0.35.

The absolute (intrinsic) permeability ( $k$ ), of the porous medium at different locations within the gas hydrate interval was measured in various core studies (as reviewed by Lewis and Collett, 2005). The estimates of effective permeability with respect to water ( $k_{ew}$ ) in Figure 3 were based on NMR-log measurements, and indicate a true (but thin) permeability



**Figure 1.** Geophysical well logs indicating the presence and saturation of gas hydrate in the thermal-test interval of the JAPEX/JNOC/GSC et al. Mallik 5L-38 gas hydrate production research well (Lewis and Collett, 2005).



**Figure 2.** Profiles of corrected porosity and total porosity in the thermal-test interval (907.0–920.0 m KB) of the JAPEx/JNOC/GSC et al. Mallik 5L-38 gas hydrate production research well (Lewis and Collett, 2005). Abbreviation: CMR, combinable magnetic resonance.

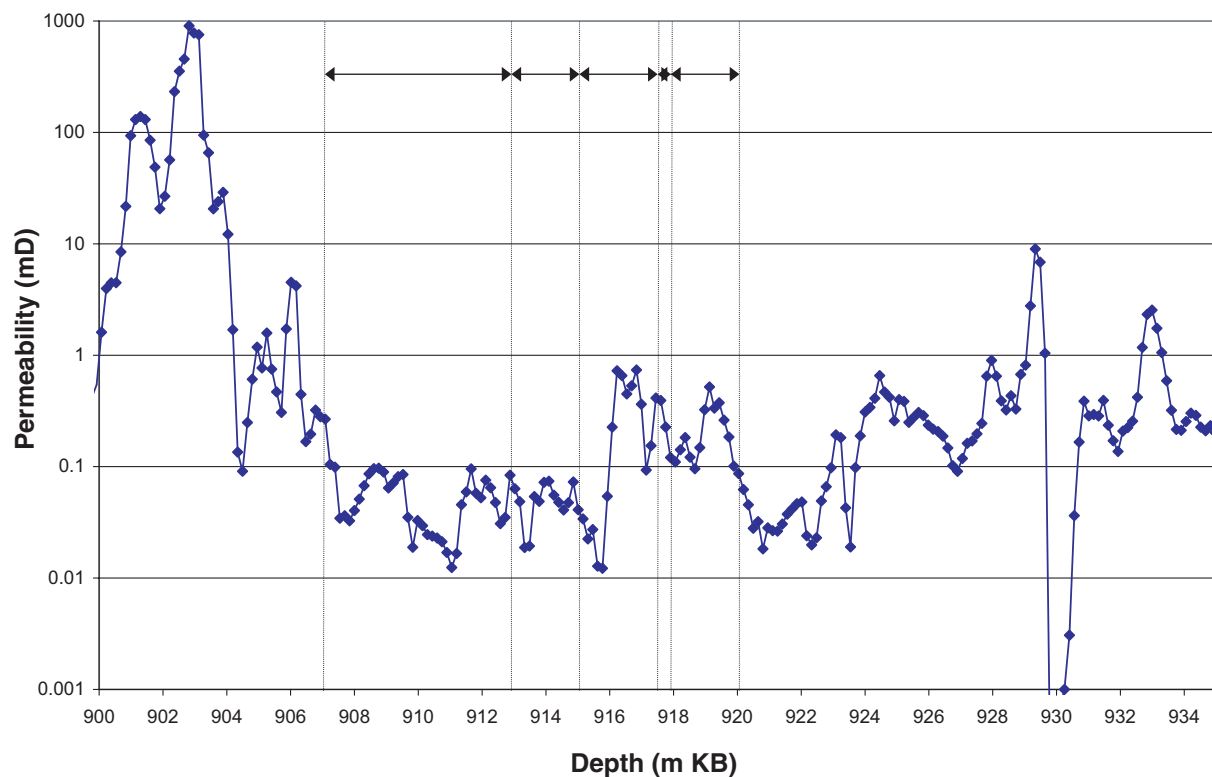


**Figure 3.** Profile of effective permeability with respect to water ( $k_{ew}$ ) in the thermal-test interval (907.0–920.0 m KB) of the JAPEx/JNOC/GSC et al. Mallik 5L-38 gas hydrate production research well (Lewis and Collett, 2005). Factors for converting permeability:  $1 \text{ mD} = 9.869 \times 10^{-16} \text{ m}^2$ , or  $1 \text{ mD} \approx 1.0 \times 10^{-15} \text{ m}^2$ .

barrier centred around a depth of 930 m (Lewis and Collett, 2005). The data in Figure 3 include the combined effects of intrinsic permeability and the effect of the presence of gas hydrate in the porous media, and were used to extract the relative permeabilities from the relationship  $k_{rw} = k_{ew}/k$ , and to determine the wettability properties (capillary pressure and relative permeability parameters).

A variant of the wettability model of Parker et al. (1987) was used to describe the relative permeability and capillary pressure functions. According to this model,

$$k_{rw} = \sqrt{\bar{S}_w} \left\{ 1 - \left[ 1 - (\bar{S}_w)^{1/m} \right]^m \right\}^2,$$

$$k_{rg} = \begin{cases} \left( 1 + \frac{k_F}{P_g} \right) \sqrt{\bar{S}_g} \left[ 1 - (\bar{S}_t)^{1/m} \right]^{2m} & \text{for } S_{gr} = 0, \\ \left( 1 + \frac{k_F}{P_g} \right) \left[ 1 - (\bar{S}_w^*)^2 \right] (1 - S_w^*)^2 & \text{for } S_{gr} > 0 \end{cases},$$

$$k_{rh} = 0$$

where  $k_{rw}$ ,  $k_{rg}$ ,  $k_{rh}$  are the relative permeabilities to water, gas, and gas hydrate, respectively;  $k_F$  is the Klinkenberg parameter (Pa) describing gas-slippage effects;  $P_g$  is the gas pressure (Pa);

$$\bar{S}_w = \frac{S_w - S_{wr}}{1 - S_{wr}}, \quad S_w^* = \frac{S_w - S_{wr}}{1 - S_{wr} - S_{gr}},$$

$$\bar{S}_g = \frac{S_g}{1 - S_{wr}}, \quad S_t = \frac{S_w + S_h - S_{wr}}{1 - S_{wr}},$$

where  $S_w$ ,  $S_g$ , and  $S_h$  are the water, gas, and gas hydrate saturations, respectively;  $S_{wr}$  ( $\approx 20\%$ ) is the irreducible water saturation;  $S_{gr}$  ( $\approx 2\%$ ) is the irreducible gas saturation; and  $m$  is a wettability parameter. The capillary-pressure function is based on the model of Parker et al. (1987), which uses the same parameters as the relative-permeability model and is given by

$$P_{cgw} = -\frac{\rho_w g}{\alpha_{gw}} \left[ (\bar{S}_t)^{-1/m} - 1 \right]^{1-m} \left( \frac{1}{1 - S_h} \right)^{1/2},$$

where  $P_{cgw}$  is the gas-water capillary pressure (Pa),  $\rho_w$  is the water density ( $\text{kg/m}^3$ ),  $g$  is the acceleration of gravity ( $\text{m/s}^2$ ), and  $\alpha_{gh}$  and  $\alpha_{gw}$  ( $\text{m}^{-1}$ ) are parameters that describe the entry pressure into the porous medium. The  $P_{cgw}$  equation involves Leverett (1941) scaling to adjust for the effect of the immobile gas hydrate phase on the ‘free’ porosity available for flow. For the sandy porous medium in the gas-hydrate-bearing interval, a value of  $\alpha_{gw} = 0.0005 \text{ m}^{-1}$  was used (Parker et al., 1987).

The parameters  $S_{wr}$  and  $m$  were determined from the  $k$  and  $k_{ew}$  estimates. These parameters are indicated in Figure 4, which shows the agreement between the model and the  $k_{rw} = k_{ew}/k$  data in layers 1, 3, and 5 of the gas-hydrate-impregnated interval. The optimum results were obtained by treating  $S_{wr}$

as a variable (dependent on the gas hydrate saturation) rather than as a constant (as is conventionally the case). Thus,  $S_{wr}$  was computed as

$$S_{wr} = S_{wr0} (1 - S_h),$$

where  $S_{wr0}$  is the irreducible water saturation in the absence of gas hydrate (assumed to be  $S_{wr0} = 0.15$  in all layers of the formation). The scientific basis for this relationship is provided by the wettability relationship between liquid water and a porous medium impregnated with gas hydrate. Because of the chemical similarity and affinity of water to gas hydrate, it is reasonable to assume that a larger gas hydrate saturation

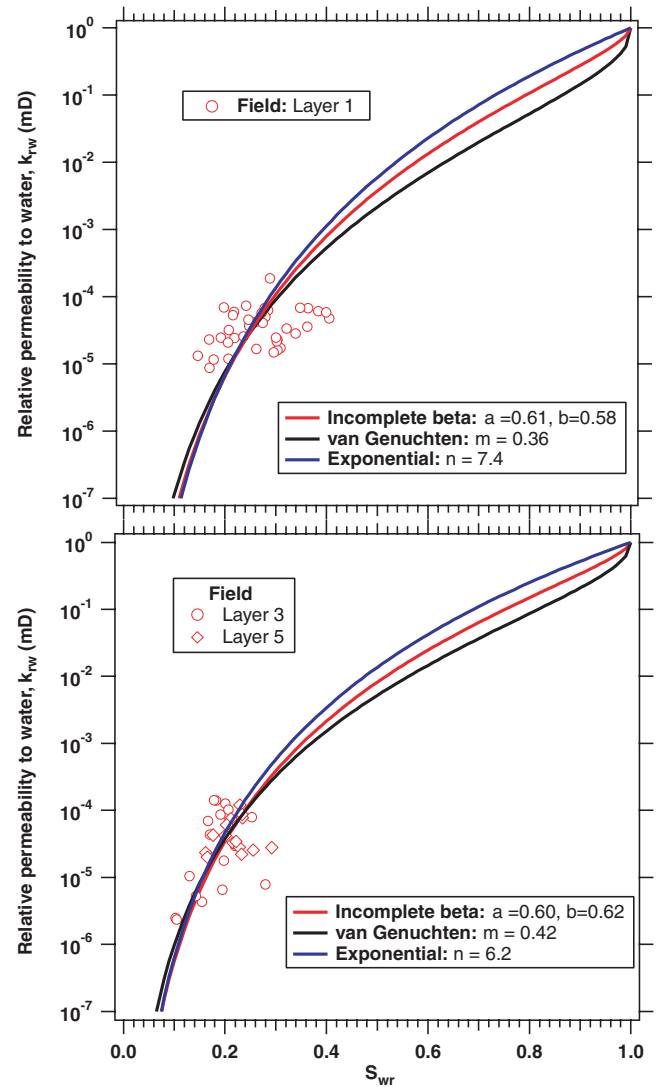


**Figure 4.** Profiles of irreducible water saturation ( $S_{wr}$ ) versus relative permeability to water, and functions used in the simulations of the thermal test in the JAPEX/JNOC/GSC et al. Mallik 5L-38 gas hydrate production research well. Factors for converting permeability:  $1 \text{ mD} = 9.869 \times 10^{-16} \text{ m}^2$ , or  $1 \text{ mD} \approx 1.0 \times 10^{-15} \text{ m}^2$ .

will correspond to a lower irreducible water saturation and consequently a larger relative permeability (and easier water flow) at lower water saturations.

Figure 4 also includes  $k_{rw}$  curves for alternative relative permeability models (included in TOUGH-Fx/HYDRATE code, but not employed in the simulations), and the best-fit estimates of the corresponding parameters. In a variant of the exponential three-phase model of Stone (1970), the relative permeabilities are computed from

$$k_{rw} = (\bar{S}_w)^n, \quad k_{rg} = \left(1 + \frac{k_F}{P_g}\right) (\bar{S}_g)^n, \quad k_{rh} = 0,$$

where  $n$  is a constant. In the incomplete beta-function model (based on the unsimplified integration of the Mualem (1976) pore-size distribution model), the relative permeabilities are given by

$$k_{rw} = \sqrt{\bar{S}_w} \left[ \frac{B(a, b, \bar{S}_w^{1/m})}{B(a, b, 1)} \right]^2,$$

$$k_{rg} = \left(1 + \frac{k_F}{P_g}\right) \sqrt{\bar{S}_w} \left[ \frac{B(a, b, 1) - B(a, b, \bar{S}_w^{1/m})}{B(a, b, 1)} \right]^2, \quad k_{rh} = 0,$$

where  $B$  denotes the incomplete beta function, and  $a$  and  $b$  are parameters. Note that the three models fit equally well the field estimates of relative permeability at the high water saturation levels of the gas hydrate interval, but their results can differ significantly at higher water saturations.

### Pressure, temperature, salinity, and distribution of gas hydrate saturation

The pressure ( $P$ ) in the gas hydrate interval matched very closely the hydrostatic pressure distribution at that depth (Hancock et al., 2005). The initial distribution of temperature ( $T$ ) was obtained from the initial (pre-test) DTS readings (Henninges et al., 2005) along the profile of the gas hydrate interval (Fig. 5). Note that the accuracy of the measurements is insufficient to resolve the minute temperature variation (estimated not to exceed  $0.4^\circ\text{C}$ ) caused by the geothermal gradient across the gas hydrate deposit in the test zone. The average initial temperature in the perforated interval was  $8^\circ\text{C}$ , substantially lower than the equilibrium hydration temperature ( $T_h$ ) of  $12.6^\circ\text{C}$ , corresponding to the prevailing pressure and a salinity of less than 10 ppt ('ppt' stands for 'parts per thousand') (as measured from core samples) at the site (Wright et al., 2005).

According to Wright et al. (2005), salinity estimates near the base of the gas hydrate stability zone ranged between 35 and 45 ppt (based on chlorinity and temperature data), and

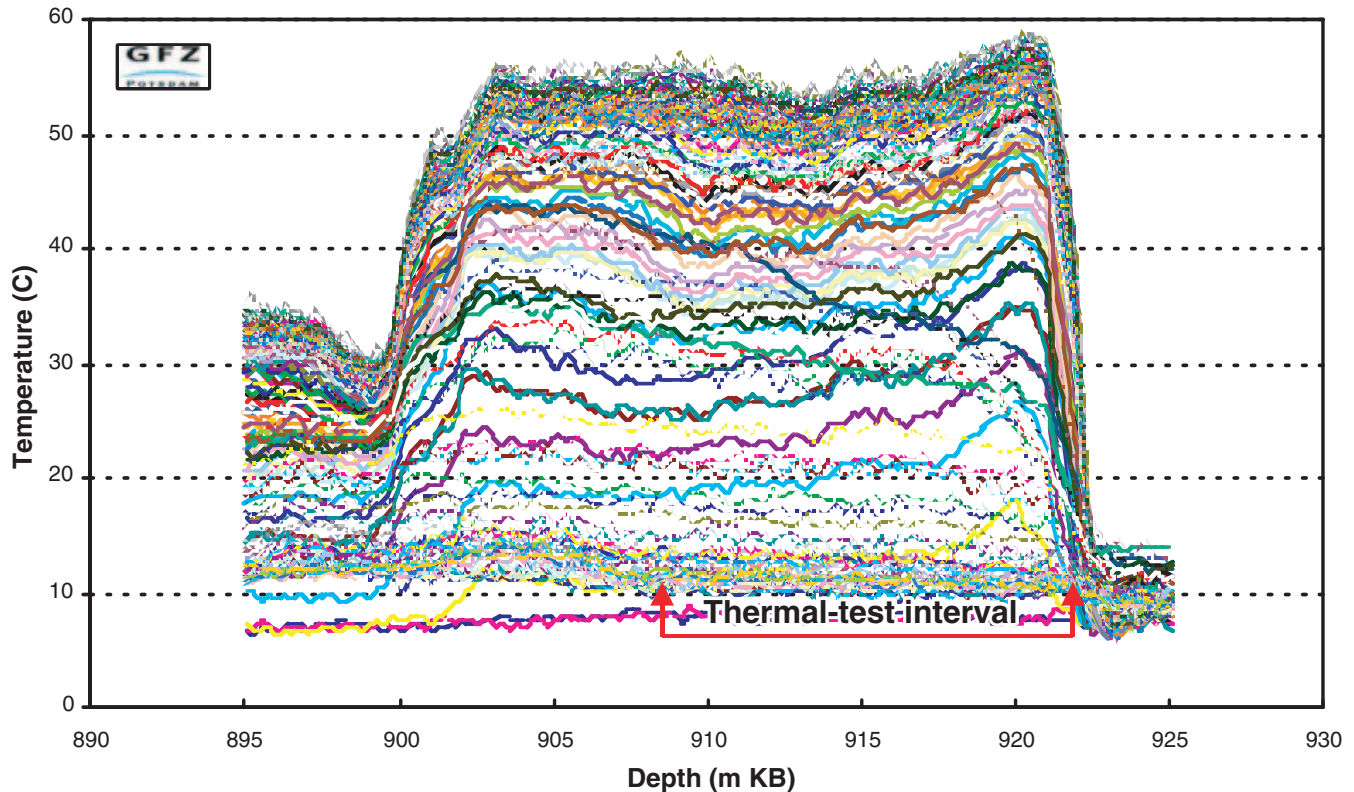


**Figure 5.** Evolution of the distributed temperature system (DTS) temperature profiles versus depth in the gas hydrate formation during the thermal test at the JAPEx/JNOC/GSC et al. 5L-38 Mallik gas hydrate production research well (Henninges et al., 2005). Readings taken at 1 hour intervals.

total salinity in the circulating water averaged 60 ppt. Considering an average initial salinity of 30 ppt, the corresponding equilibrium hydration temperature ( $T_h$ ) was expected to be lower than that of pure water by about 1.7°C (Wright et al., 1999). This downward shift in  $T_h$  made dissociation easier.

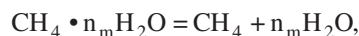
The gas hydrate saturations ( $S_h$ ) in the gas hydrate test interval (906–924 m) in Figure 6 are nonuniform (Lewis and Collett, 2005). In terms of the layers identified in Figure 2,  $S_h$  is highest in layers 3 and 5, and lower in the lower porosity layers 2 and 4. In general, the gas hydrate saturation is high in the well-log- and core-inferred gas-hydrate-bearing intervals (exceeding 70% on average), making this an attractive production test target. The remainder of the pore space is occupied by water.

## NUMERICAL MODEL

### Numerical simulator

The numerical studies of gas production in this paper were conducted using the TOUGH-Fx/HYDRATE model, a successor to the TOUGH2/EOSHYDR2 model (Moridis, 2003). The TOUGH-Fx/HYDRATE model represents the new generation of the TOUGH2 family of codes (Pruess et al., 1999) for multicomponent, multiphase fluid and heat flow and transport in the subsurface. By solving the coupled equations

of mass and heat balance, TOUGH-Fx/HYDRATE models the behaviour of methane hydrate that forms or dissociates in porous media according to the general reaction equation



where  $n_m$  is the hydration number of the methane hydrate, which can range between 5.75 and 7.2 (Sloan, 1998). The TOUGH-Fx/HYDRATE model includes both an equilibrium and a kinetic model of gas hydrate formation and dissociation, and can describe gas hydrate dissociation involving any combination of the possible dissociation mechanisms (i.e. depressurization, thermal stimulation, and inhibitor effects). A detailed description of TOUGH-Fx/HYDRATE can be found in Moridis (2004b).

### Simulation domain

A schematic diagram of the simulation domain with a simplified description of the thermal test is depicted in Figure 7. Both the wellbore and the relevant subsurface formations (including the gas-hydrate-bearing interval and its confining boundaries) are represented in the cylindrical simulation domain. In the numerical representation of the thermal-test domain, impermeable flow boundaries were assumed to confine the gas hydrate interval (depicted as shale layers in Figure 7) at 906 and at 925 m. Although the corresponding confining shale zones at these elevations had low (but nonzero) intrinsic

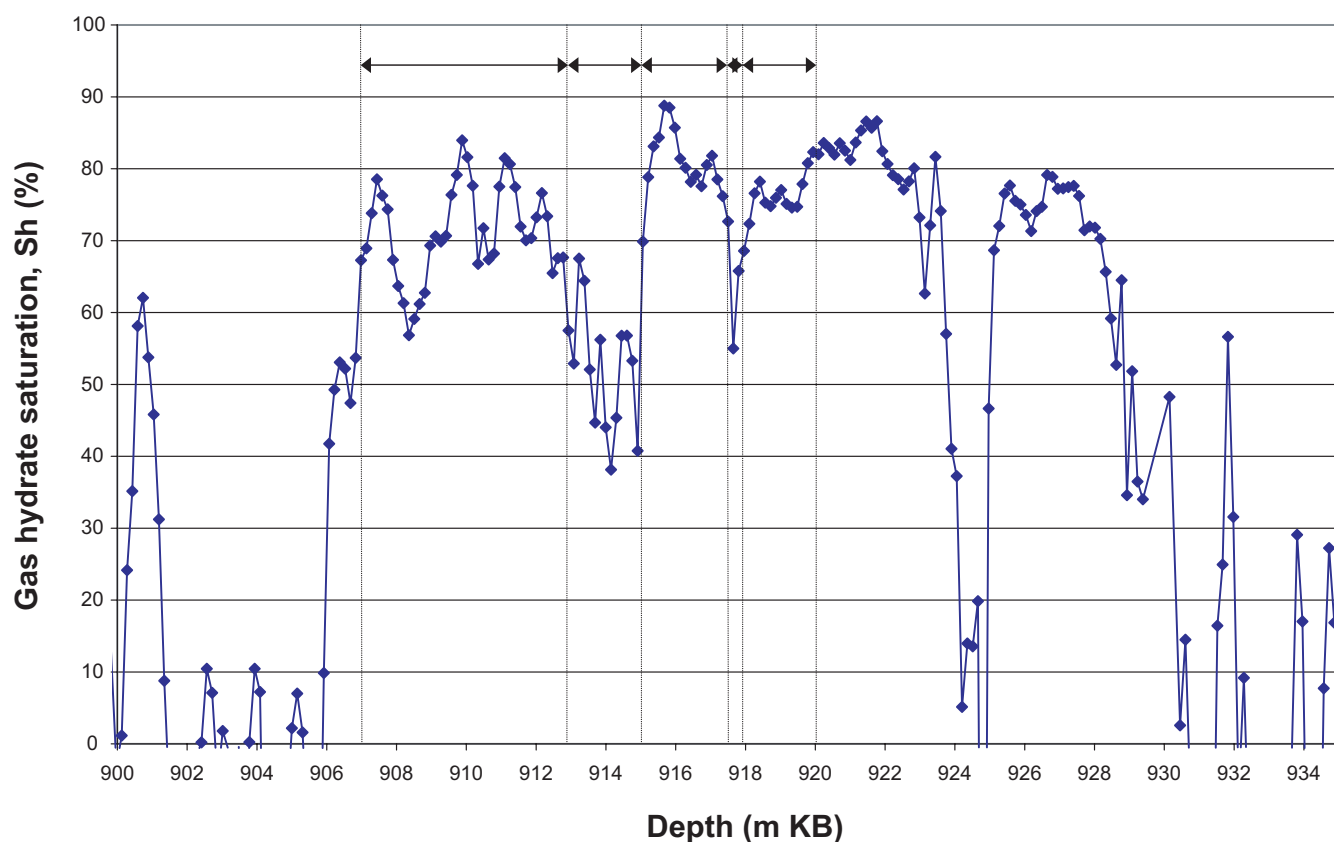


**Figure 6.** Profile of gas hydrate saturation ( $S_h$ ) in the thermal-test interval (907.0–920.0 m KB) of the JAPEX/JNOC/GSC et al. Mallik 5L-38 gas hydrate production research well (Lewis and Collett, 2005).

permeability, the assumption of impermeable boundaries was reasonable given the much larger intrinsic permeability of the hydrate zone and the need to keep the size of the problem manageable.

The top flow boundary coincides with the end of the gas hydrate. Although the geophysical-well-log data of Figure 1 indicate that, with an exception of a very thin zone at 926 m, the gas hydrate interval continues to a depth of 930 m, the placement of the boundary for bottom flow at 925 m is a valid approximation designed to minimize the size of the numerical problem to be solved. This is supported by the DTS temperature profile in Figure 5, which does not indicate any significant changes below 923 m and provides evidence that this portion of the gas hydrate interval was inactive during the thermal test (thus justifying the assumption of a bottom boundary at 925 m). The analysis of the conventional-log data (Anderson et al., 2005) also indicates that the depth interval from 906 to 925 m was affected by the thermal-stimulation test.

Based on earlier scoping calculations (Moridis et al., 2004), the cylindrical simulation domain extended to a radius ( $r_{\max}$ ) of about 10 m, which had been determined to be sufficiently large to accommodate the spatial extent of the dissociation zone and of the flow processes and changes occurring during the thermal test. Because of an initial water saturation at or near the irreducible  $S_{wr} = 0.2$ , negligible flow and pressure change were expected at the  $r_{\max}$  boundary. Thus, a

constant-pressure (Dirichlet-type) boundary was assumed at  $r = r_{\max}$ . Although the scoping calculations had indicated that the thermal front would not be advancing past the  $r_{\max}$  boundary, this study used a TOUGH-Fx/HYDRATE option that computes correct heat fluxes at the impermeable boundary by employing an accurate analytical solution based on a semi-infinite temperature boundary. In the  $z$  co-ordinate, the simulation domain spanned the 904 to 927 m interval (i.e. it was extended 2 m above and below the boundaries of the gas-hydrate-bearing interval). This was necessary to accurately describe the heat fluxes through the impermeable flow boundaries. Simple thermal studies using analytical solutions of heat transfer had indicated that the 2 m extension of the domain on either side of the gas hydrate interval was sufficient to provide a constant-temperature boundary during the relatively short duration of the thermal test.

The domain was discretized into 250 by 72 subdivisions in ( $r, z$ ), resulting in a total of 18 000 active grid blocks. This fine discretization ( $\max\{\Delta r\} = 0.05$  m,  $\max\{\Delta z\} = 0.2$  m in the simulated formations) was chosen to eliminate potential spatial-resolution problems and accurately describe the pressure and temperature gradients during the thermal test. Note that the geometry of all the different subdomains in the wellbore vicinity (injection tube, annular space, well casing, cemented interval, steel packer) was accurately represented in the simulation domain (Hancock et al., 2005).

For the scoping calculation of long-term production under a variety of scenarios, the discretization along the  $r, z$  axes and the total number of grid blocks remained the same, but the grid-block size increased to accommodate the expanding flow and thermal boundaries of the system. Thus, for the three-year production simulations discussed in a subsequent section,  $r_{\max}$  was increased to 100 m, the full gas hydrate interval (from 906 to 930 m) was considered, and the thermal boundaries were extended to 20 m past the flow boundaries. Because of the longer simulation period, the grid (coarser than the one for the short-term thermal-test simulation but still fine in absolute terms) was capable of accurately describing the simulated processes.

### Simulated processes and phenomena

The following processes and phenomena occurring during the thermal test were considered in the simulations:

- gas hydrate dissociation
- gas dissolution in the water
- fluid flow (water and gas)
- salt dilution (caused by the water released during dissociation) and transport (advection, diffusion, and dispersion)
- effects of changes in pressure, temperature, and salinity on dissociation
- thermal effects, including heat of dissociation, heat of dissolution, phase changes, and heat transport (through fluid flow and conduction)

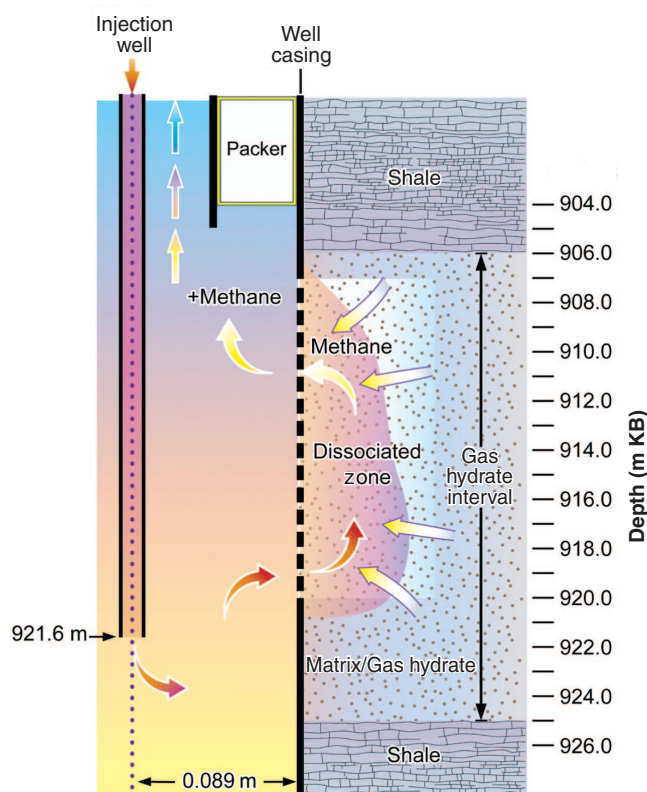


**Figure 7.** Schematic diagram of the simulation domain of the thermal test, JAPEX/JNOC/GSC et al. Mallik 5L-38 gas hydrate production research well.

The gas hydrate dissociation was treated as both an equilibrium and a kinetic process. In simulations involving thermal stimulation (i.e. thermal stimulation only or combined with depressurization) under equilibrium dissociation, the inclusion of the phases, mass components, heat, and the processes described above necessitated the solution of four coupled equations per grid block (corresponding to heat and the water, methane, and salt components). In thermal-stimulation simulations under a kinetic-dissociation regime, the number of coupled equations per grid block was five, with the solid gas hydrate being the additional mass component. Thus, the order of the Jacobian matrix (Pruess et al., 1999) ranged from 72 000 to 90 000.

### Data inputs, parameters, and conditions

The hydraulic and wettability properties of the gas-hydrate-bearing formation used in the simulations were as previously described. Thus, the  $k$  estimates from core studies (averaging about  $2 \times 10^{-13} \text{ m}^2$ ), and the relative permeability and capillary pressure curves of the model employed by Parker et al. (1987), were used (see Fig. 4) for layers 1, 3, and 5. In the absence of direct  $k$  measurements for layers 2 and 4, the relative permeability function for layer 1 was used, and  $k$  was estimated from the gas hydrate saturation  $S_h$  (Fig. 6) and the effective permeability  $k_{ew}$  (Fig. 3) in these layers. Initially, the average porosities in the five layers (Fig. 3) were used, and small adjustments were made in individual layers or grid blocks during history matching. A porosity ( $\phi$ ) of 2% was assigned to the impermeable flow boundaries. Although this value appears to be in conflict with more recent estimates of  $\phi$  (20%, inferred from density logs), it does not pose a problem for the simulation results because permeability (not porosity) is the only parameter affecting the boundary behaviour. Although it is possible that the bounding siltstone was not completely impermeable, it was assumed that it acted as such because of 1) the very large disparity between its permeability and that of the gas hydrate test interval, and 2) the expected preferential gas flow toward the very permeable wellbore.

The thermal properties of the matrix of the gas hydrate interval and of its boundaries were assumed to be uniform. This is a good approximation because the thermal properties of rocks are known to be far more uniform than their hydraulic properties. The initial specific heat of the rock ( $C_R$ ) was  $1000 \text{ J/kg/}^\circ\text{C}$ , and the corresponding thermal conductivity ( $\kappa_R$ ) was  $2.5 \text{ W/m/}^\circ\text{C}$ . Note that  $C_R$  and  $\kappa_R$  are perturbation parameters to be determined through the history-matching process.

The thermophysical properties of water used in the simulations were provided by the steam tables incorporated in all members of the TOUGH2 family of codes (Pruess et al., 1999; Moridis, 2003). The hydrocarbon in the gas hydrate was assumed to be 100% methane. This is a valid approximation, one supported by gas analysis evidence from cores, which has indicated the gas to be at least 98% methane (Tulk et al., 1999; Wiersberg et al., 2005; Lorenson et al., 2005). The thermophysical properties of methane were obtained using the Peng-Robinson equation of state for real gases incorporated into the TOUGH-Fx/HYDRATE model (Moridis, 2004b).

The initial values of the specific heat ( $C_h$ ) and thermal conductivity ( $\kappa_h$ ) of the gas hydrate (also perturbation parameters to be determined through history matching), as well as the density ( $\rho_h$ ), were provided by methane hydrate data reported in Sloan (1998) as  $2078 \text{ J/kg/}^\circ\text{C}$ ,  $0.45 \text{ W/m/}^\circ\text{C}$ , and  $920 \text{ kg/m}^3$ , respectively. The composite thermal conductivity ( $\kappa_l$ ) of the gas-hydrate-impregnated medium was computed from the parallel model of Bejan (1984) as

$$\kappa_l = (1 - \phi)\kappa_R + \phi S_w \kappa_w + \phi S_g \kappa_g + \phi S_h \kappa_h,$$

where  $\kappa_w$ ,  $\kappa_g$ , and  $\kappa_h$  are the thermal conductivities of water, gas, and gas hydrate, respectively.

The initial hydration number ( $N_H$ ) was assumed to be 6.0, consistent with reported literature values (Sloan, 1998). The relationship between the hydration equilibrium pressure and temperature (for pure water), and the dependence of the heat of dissociation ( $\Delta H$ ) on temperature were provided by modifications of the equations developed by Moridis (2003) and are presented in Figures 8 and 9. The original effect of salinity on the dissociation equilibrium pressure-temperature relationship was described by the equation

$$T_s = \left[ \frac{1}{T_H} - \frac{n_m \Delta H^f}{\Delta H} \left( \frac{1}{273.15} - \frac{1}{T_f} \right) \right]^{-1},$$

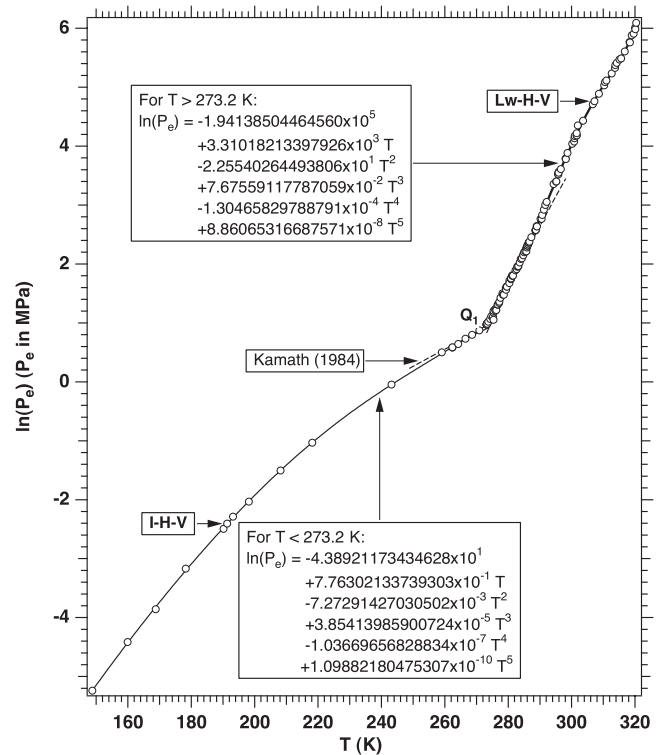


**Figure 8.** Pressure-temperature relationship at gas hydrate equilibrium (Moridis, 2003). Laboratory measurements and the relationship of Kamath (1984) are included for reference. Abbreviations: H, gas hydrate; I, ice; Lw, liquid water;  $P_e$ , equilibrium hydration pressure (in Pa); V, vapour.

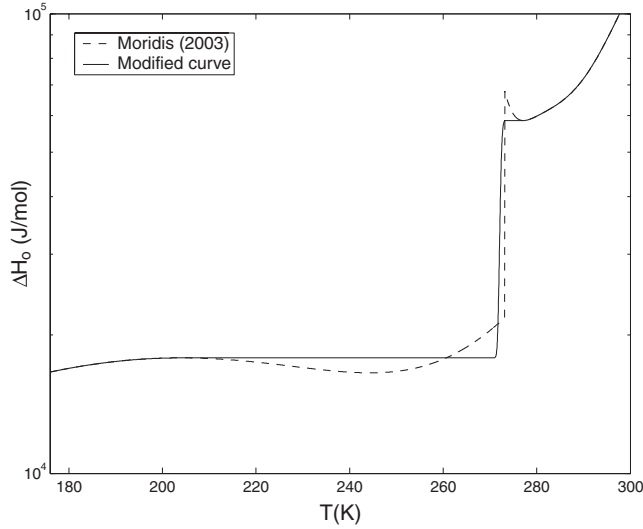


**Figure 9.** Dependence of enthalpy of gas hydrate dissociation on temperature in the TOUGH-Fx/HYDRATE code. The modified curve used in the TOUGH-Fx/HYDRATE simulations reflects corrections in the Moridis (2003) curve to account for density differences in the Clausius-Clapeyron equation.

reported in Sloan (1998). In this equation,  $T_s$  is the equilibrium dissociation temperature in the salt solution (K),  $\Delta H^f$  is the heat of fusion of ice (J/kg),  $T_H$  is the equilibrium dissociation temperature in the presence of pure water (K), and  $T_f$  is the freezing point of the salt solution (K). The predictions of this equation are in broad agreement with the measurements of Wright et al. (1999). Further analysis allowed the above complex equation to be replaced with the simpler and equally accurate relationship

$$\Delta T_D = \Delta T_{D,r} \frac{\ln(1-x)}{\ln(1-x_r)},$$

where  $\Delta T_D = T_s - T_H$ ,  $x$  is the mole fraction of the salt in the liquid phase, and  $\Delta T_{D,r}$  is the temperature depression at a reference mole fraction  $x_r$ . Note that the above equation can be used both for salts and for water-soluble inhibitors, such as alcohols.

The rate of kinetic dissociation was estimated, using the equation of Kim et al. (1987), as

$$Q = K_d^0 \exp\left(\frac{\Delta E}{RT}\right) A [f_g(T) - f_g],$$

in which  $K_d^0$  is the intrinsic dissociation rate constant ( $\text{mol}/\text{m}^2 \cdot \text{Pa} \cdot \text{s}$ ),  $\Delta E$  is the activation energy for gas hydrate dissociation (J/mol),  $R$  is the universal gas constant (8.314 J/mol/K),  $T$  is the temperature (K),  $A$  is the surface area of the dissociating gas hydrate ( $\text{m}^2$ ), and  $f_g$  and  $f_g(T)$  are the fugacities (Pa) in the gas phase and at hydration equilibrium at a given temperature, respectively. The term  $A$  does not remain constant, but changes with the gas hydrate saturation.

The surface area is computed by assigning the hydrate saturation uniformly to the interstitial spaces of the porous medium. To accomplish this, the original solid-grain volume (considered to be composed of spherical particles) is determined as  $V_p = 4\pi r_p^3/3$ , where  $r_p$  is the solid-grain radius. Then, the number of voids  $N_V$  (pore spaces) is assumed to be equal to the number of solid grains (a valid approach for spherical particles), and the corresponding void volume  $V_V$  is computed from

$$N_V = \frac{(1-\phi)}{V_p}, \quad V_V = \frac{\phi}{N_V}.$$

At the interface of pores and voids, the grain surface area is the same for both the grains and the voids, and is computed as  $A_p = 4\pi r_p^2$ , resulting in a total area (per unit volume) of  $A_{TV} = N_V A_p$ . The volume of the void is assumed to vary linearly with  $r_V^3$ , where  $r_V (= 0.1547 r_p)$  is a representative radius describing the radius of the sphere fitting in the interstitial space between the spherical grains. Then, at any time  $t$ , the representative hydrate ‘particle’ radius  $r_h$  and volume  $V_h$  are computed as

$$V_h = \frac{\phi S_h}{N_V}, \quad r_h = r_V \left( \frac{V_h}{V_V} \right)^{1/3} = r_V S_h^{1/3},$$

and the corresponding hydrate reactive area is computed as

$$A = f_A A_{TV} \left( \frac{r_h}{r_V} \right)^2 = f_A N_V \left( \frac{4}{3} \pi r_p^3 \right) S_h^{2/3},$$

Given the intrinsic permeability ( $k$ ) of a porous medium, the Kozeny-Carman equation can provide an estimate of the average (effective) radius of the porous medium grains ( $r_p$ ) as (Bear, 1972)

$$r_p = \left[ 45k \frac{(1-\phi)^2}{\phi^3} \right]^{1/2},$$

Alternatively, an estimate of  $r_p$  can be obtained from sieve analysis (if such data are available). The area adjustment factor  $f_A$  accounts for the deviation of the interstitial volume from that based on the assumption of grain sphericity, and can incorporate heterogeneity effects related to the hydrate ‘particle’ size and distribution.

Given the design of the thermal test, the  $T$  and  $P$  data collected during the thermal test cannot be used for calibration and history matching because 1) the DTS-based  $T$  measurements were made very close to the circulating water boundary, and 2) the  $P$  measurements lacked sufficient spatial definition (i.e. they were made at a single location within the wellbore). The  $P$  and  $T$  data, however, provided the necessary boundary conditions at the well. In the validation simulations of the thermal test, a variable-pressure boundary was attached to the top of the domain (at a depth of 904 m), in the space between the packer and the inner injection tube (Fig. 7). The pressure in this boundary grid block was that from the downhole measurements (Fig. 10), corrected for the hydrostatic pressure difference between the elevations of the gauge (at 874.4 m) and the centre of the boundary grid block (at 903.95 m). Hot

water was injected directly into the grid block corresponding to the bottom of the hot-water-injection inner tube (at 923.6 m, Fig. 7) at the variable rate obtained from the test operational logs. The temperature of the injected water was that of the DTS measurements for the 918 to 921 m zone (Fig. 11), adjusted to account for the distance and location of the DTS cable. The adjustment involved a temperature increase of 0.6°C, determined by means of an interactive simulation.

### Validation approach and parameter estimation

The validation approach centred on the ability to numerically reproduce the field observations by varying simulation parameters (describing the processes occurring during the thermal test) within reasonable limits. This approach incorporates the concept of calibration. The only data set suitable for the purpose was the volume of produced gas. Because the test was conducted on a Class 3 gas hydrate accumulation (Moridis and Collett, 2003) with no underlying zones of mobile fluids, all the produced gas had originated from gas hydrate.

The inverse modelling (history-matching) process sought to minimize the deviations between the TOUGH-Fx/HYDRATE predictions and the produced gas volume, using the method of Thomas et al. (1972). Several parameters (discussed in the 'Parameter determination and general observations' section), were perturbed during history matching, including the intrinsic

permeability, porosity, and initial gas hydrate saturation of select subdomains; the gas hydrate thermal properties; and the hydration number. The most sensitive ones (identified early) were selected as perturbation parameters, and their final values (which minimized the difference between measurements and predictions) were determined after several iterations.

### VALIDATION AND PARAMETER ESTIMATION

Two different approaches were employed in the effort to validate the model against the results of the thermal test at the Mallik 5L-38 well. The basis of the first approach was fidelity to the data on released-gas volumes (unadjusted data) collected during the 125 hours of hot-water circulation in the well. The underlying assumption in this approach was the correctness of all the points in the data set. The basis of the second approach was fidelity to the overall trend during the evolution of released-gas volumes over time. In this case, the study was based on the thesis that, while there may exist uncertainty over individual data points, the averaged values (time-averaged smoothed data) and the overall trend are correct. In each validation approach, the data were analyzed by employing both an equilibrium and a kinetic gas hydrate dissociation model.

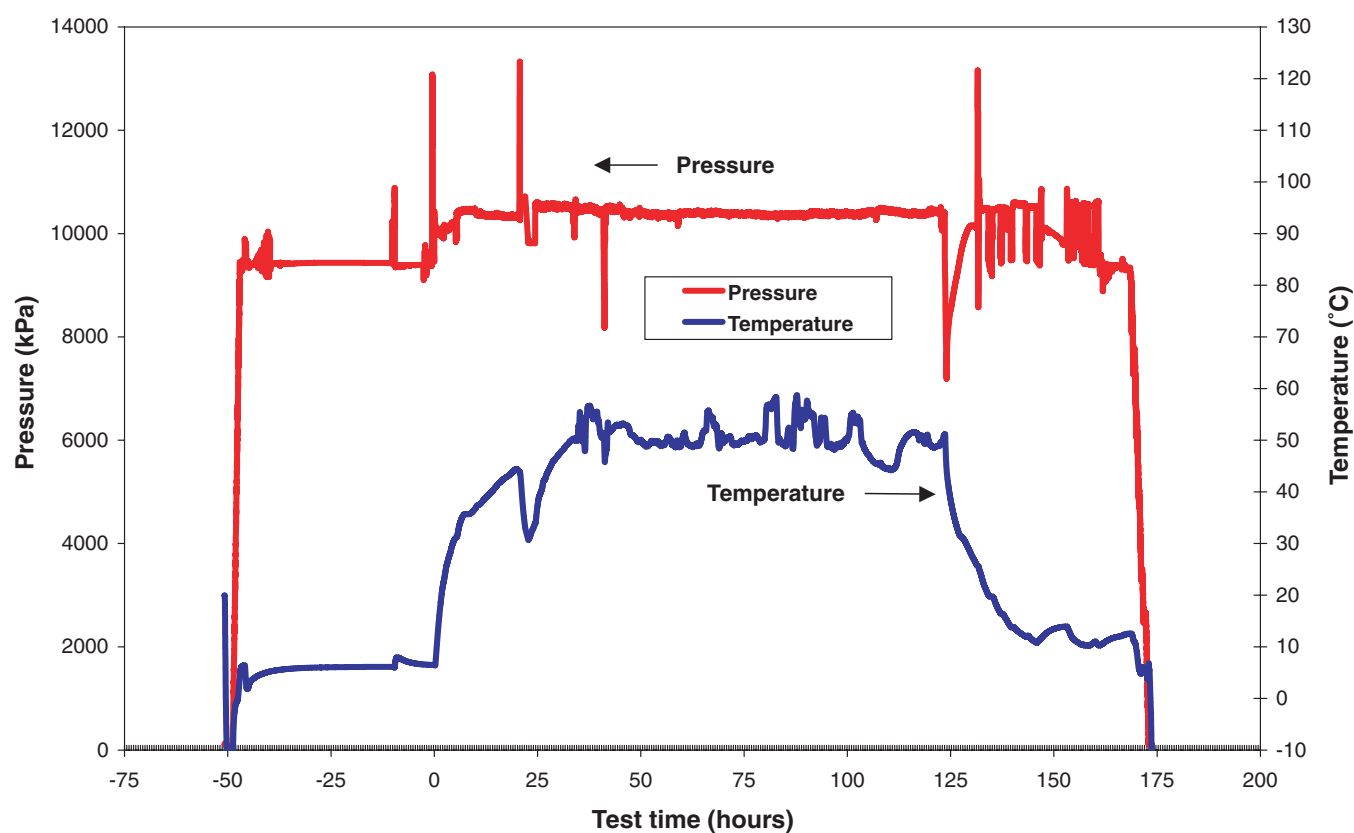


**Figure 10.** Downhole-pressure and -temperature measurements (taken with Weatherford EMR Quartz Gauge #5013 at 876.4 m KB) during the thermal test in the JAPEx/JNOC/GSC et al. Mallik 5L-38 gas hydrate production research well (Hancock et al., 2005).

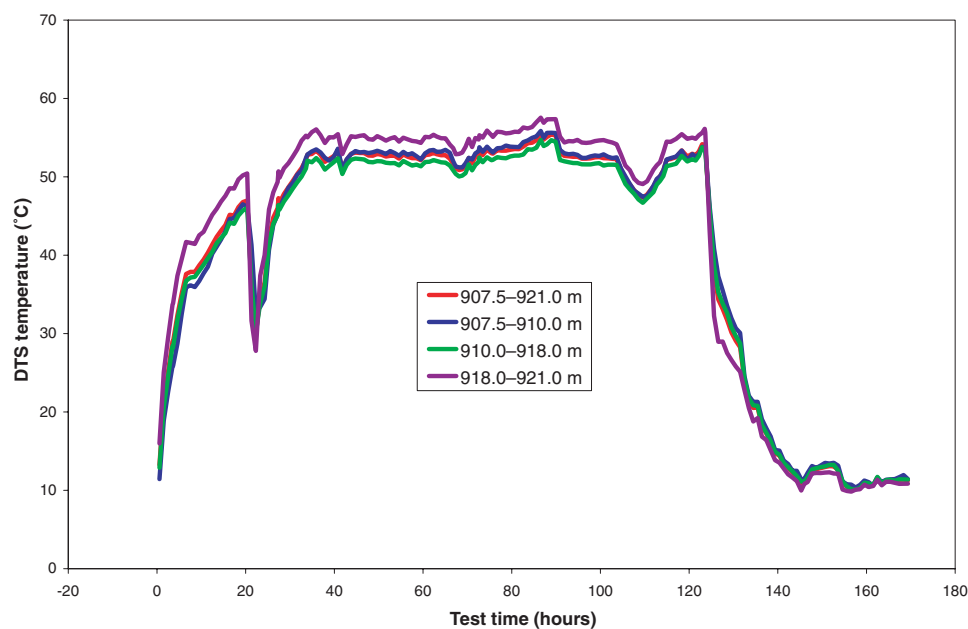


**Figure 11.** Distributed temperature system (DTS) temperature profiles at various segments of the gas-hydrate-bearing formation during the thermal test in the JAPEx/JNOC/GSC et al. Mallik 5L-38 gas hydrate production research well (Hancock et al., 2005).

### Validation assuming fidelity to data

#### Concept of the gas hydrate fracture zone

In the effort to match numerical predictions and the volume of produced gas, the concept of the gas hydrate fracture zone was introduced when fidelity to data was assumed (unadjusted data). It involved the assumption of a narrow cylindrical zone that surrounds the perforated interval at the well and is characterized by microfractures. Consideration of such a zone was an important component in the effort to accurately reproduce the field observations.

There is strong scientific justification (and anecdotal evidence from laboratory experiments) for assuming the creation of a fracture zone in the immediate vicinity of the wellbore in a previously undisturbed gas-hydrate-bearing formation. These microfractures are created as the temperature of the circulating water at the well rises rapidly, leading to thermal and pressure shocks (Perkins and Gonzalez, 1985), specifically sharp thermal gradients, sudden pressure build-ups caused by fast gas release at the dissociation front, and accumulation of thermal and mechanical stresses. Preliminary estimates of the fracturing pressure of gas hydrate at the Mallik site (ranging between 7 and 17 MPa) do not appear to contradict the assumption of a microfracture zone.

Such microfractures are presumed to be akin to those caused by thermal shock when ice cubes come in contact with hot water (Frost, 2001), and have been observed in gas hydrate samples in unreported experiments conducted at the United States Geological Survey (S. Kirby, pers. comm., 2004), the National Energy Technology Laboratory (T. Mroz, pers. comm., 2004), and the Lawrence Berkeley National

Laboratory (T. Kneafsey, pers. comm., 2004). In the case of gas hydrate, microfracturing is expected to be enhanced by the rigorous volume expansion of the released gas. Although this hypothesis has yet to be rigorously tested, the emergence of a fracture network that releases the thermomechanical stresses appears to be a reasonable assumption. The extent of the fracture zone is limited because such a rapid stress accumulation occurs only during the early stages of the hot-water circulation, when the pressure and thermal gradients have been shown to be very steep (Fig. 12). At later times, the thermal and pressure gradients become increasingly shallower, allowing stress release over progressively larger volumes and falling below the fracturing threshold.

The fractured system in the well vicinity is described mathematically by the 'dual-permeability' concept (Warren and Root, 1963; Pruess, 1991), which involves interacting matrix and fracture continua (Fig. 13). Each of these two components has its own separate hydraulic and wettability properties ( $\phi$ ,  $k$ ,  $k_{rw}$ ,  $k_{rg}$ ,  $P_{cwg}$ ). Fluid flows occur through matrix-to-matrix, matrix-to-fracture, and fracture-to-fracture interactions. Immediately upon fracturing, gas hydrate is confined to the matrix, while the fractures are occupied by water and gas from gas hydrate dissociation. The results of the fractured zone are an increased permeability and enhanced gas dissociation because of 1) the increased surface area exposed to the advancing hot water, and 2) the existence of a more extensive pathway system for gas release.

In the simulations for the thermal-test validation, the fracture zone extended to a radius ( $r$ ) of 0.47 m, and was determined through an iterative trial-and-error process. During the same process, the fracture aperture was determined to be 50  $\mu\text{m}$ ,

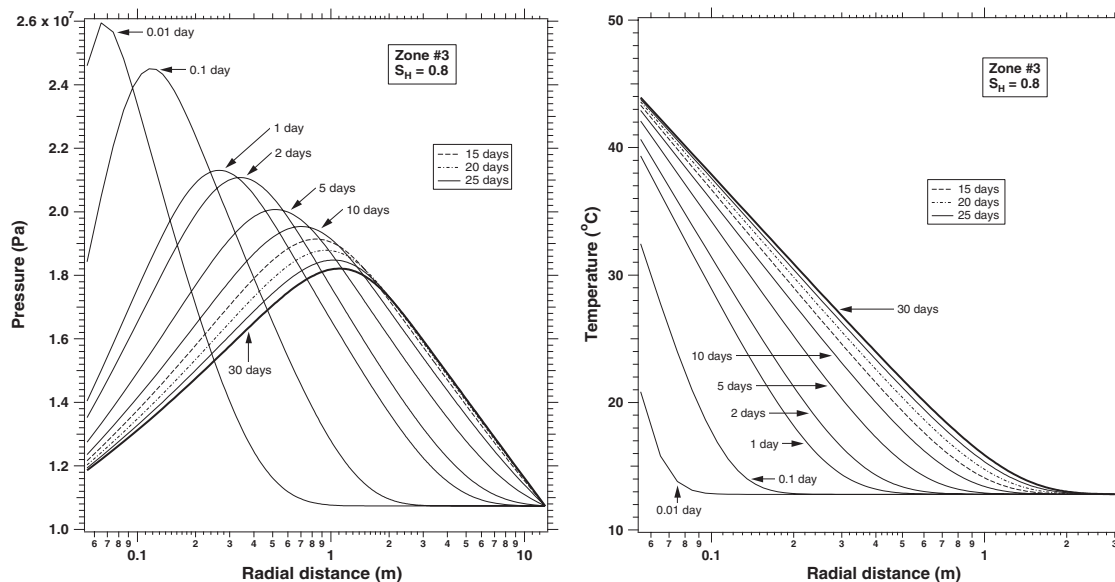


**Figure 12.** Pressure and temperature distributions as gas hydrate is exposed to 50°C water (Moridis et al., 2004), JAPEx/JNOC/GSC et al. Mallik 5L-38 gas hydrate production research well. Note the steep gradients at early times.

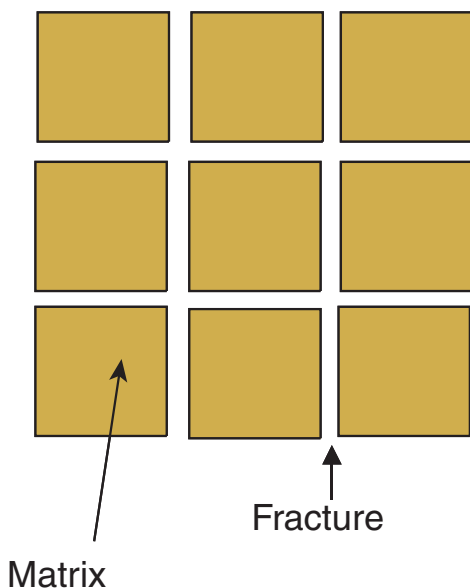


**Figure 13.** Schematic diagram of the 'dual-permeability' concept used to describe the gas hydrate fracture zone.

and the matrix block size was 2 to 5 cm. Note that the fracture permeability was determined from the aperture  $b$  using the relationship  $k_f = b^3/12$  (de Marsily, 1986), and the relative permeability and capillary pressure functions were described by the equations of Parker et al. (1987), with parameters obtained from scaling of the matrix parameters using the Leverett J-function (Leverett, 1941).

Three periods can be identified in the course of the thermal test. In the short initial period, the water temperature at the well was low and rising, but insufficient to cause fracturing. The second period was also relatively short and was characterized by near-well fracturing of the gas-hydrate-bearing formation, caused by a rapid increase in water temperature and sudden gas releases. No fracturing occurred in the third 'stability' period, which was the longest and was characterized by mild, diffuse temperature and pressure gradients. The gas production pattern during the field test (Fig. 10) is attributed to the different dissociation and flow characteristics during each of the three periods.

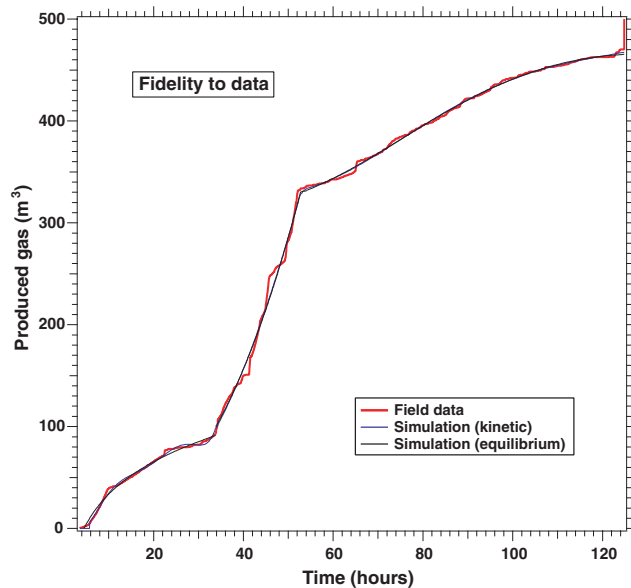
### Results of the history-matching process

Figure 14 shows the evolution of the numerically predicted, cumulative volumes of released gas over time during the first 124.8 hours of the thermal test for both equilibrium and kinetic dissociation, in addition to the corresponding measured data. The numerical results in Figure 14 correspond to the optimal values of the perturbation parameters (presented and discussed in the 'Parameter determination and general observations' section), which were determined through history matching as those that minimized deviations between predictions and observations.

Comparison of the three curves indicates a very good agreement. The results for kinetic and equilibrium dissociation are practically indistinguishable. Note that the three distinct segments (characterized by different slopes) of the curves correspond to the three dissociation periods identified in the previous section. Of particular interest is the second

segment, which corresponds to the microfracturing of the gas-hydrate-bearing formation and is characterized by fast gas release.

The distribution of gas hydrate saturation at the end of the period of hot-water circulation ( $t = 124.8$  hours) is shown in Figure 15, which indicates 1) a zone of high gas saturation in



**Figure 14.** Comparison of measurements and numerical predictions (using calibrated parameters) in the validation attempt that assumes fidelity to data (unadjusted measurements are used), JAPEx/JNOC/GSC et al. Mallik 5L-38 gas hydrate production research well.

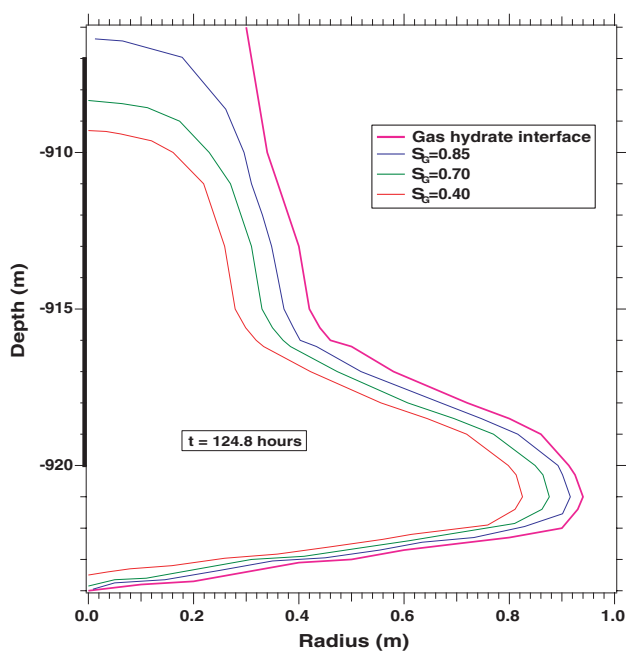


**Figure 15.** Numerically predicted gas hydrate saturation distribution at the end of the thermal test, JAPEx/JNOC/GSC et al. Mallik 5L-38 gas hydrate production research well.

contact with the dissociating gas hydrate interface, and 2) a gas hydrate dissociation that is far more extensive in the lower part of the formation. This is consistent with expectations, because buoyancy tends to lead to gas accumulation toward the upper part of the formation, where a layer of gas hugging the gas hydrate interface (as it flows toward the well) is formed. This preferential gas accumulation leads to reduced overall thermal conductivity and increased specific heat in the zone of high gas saturation, which in turn limits the amount of heat reaching the interface and reduces dissociation. The validity of these predictions is supported by the estimates of the dissociation zone deduced from geophysical well logs (Anderson et al., 2005), which provide evidence of significantly more extensive dissociation in the lower part of the gas-hydrate-bearing formation. Figure 15 also indicates gas accumulation in the space between the top of the perforation interval and the upper flow boundary, a scenario supported by the geophysical-well-log data of Figure 1 (Anderson et al., 2005; Lewis and Collett, 2005).

The limited extent of the dissociation zone in Figure 15 is evidence of the inefficiency of hot-water circulation as the sole dissociation method for gas production. Under these conditions, heat is transported through conduction and advection. Conduction is a slow and inefficient process, and is adversely affected by the evolution of the zone of released gas that hugs the gas hydrate interface as it flows toward the well. In addition to the very large thermal inertia of the porous medium, this zone is adversely affected by the lower conductivity to water and higher specific heat of the gas. As is indicated by analysis of the pressure distribution in the vicinity of the gas hydrate interface, advective heat transport is lessened by the emergence of a high-pressure ridge. This high pressure is caused by the dissociation-induced gas release; is oscillatory (as gas and pressure first build up and are then released); can lead to temporary flow stagnation as the released gas collides with the advancing hot-water front (Fig. 16); and reduces direct contact of the water with the gas hydrate. Additionally, the high-pressure ridge can also result in gas flowing away from the interface into the gas-hydrate-bearing formation (if permitted by the permeability conditions), limiting the volume of gas reaching the well.

#### Validation assuming fidelity to the smoothed data trend

In this approach, history matching was applied against not the individual data points but a general 'average' curve that is faithful to the overall trend of cumulative gas production. No gas hydrate fracturing was considered in this case. Two different scenarios, A and B, were studied in this approach. The difference between the two is the inclusion in the data set of an additional volume of gas (released immediately after the cessation of water circulation) in scenario B.

Comparison of the measured volumes and the numerically predicted results (for the optimal parameter values determined from history matching) shows good agreement for both scenarios. The differences in the predictions for equilibrium and kinetic dissociation in scenario A are consistent with expectations. Thus, released volumes are initially larger

for equilibrium dissociation (an instantaneous process compared to the slower kinetic process), but their differences vanish at longer times.

Because of the ability to determine parameters that result in similar performances for both equilibrium and kinetic dissociation, only equilibrium dissociation was considered in scenario B (depicted in Fig. 17). Note that, as in all previously discussed cases, the intense conditions of thermal stimulation support the thesis that, under the conditions of the thermal test, dissociation caused by the advancing hot-water front coming in contact with the hydrate is a fast process, in which case the equilibrium model is a good approximation of the kinetic model. For circulating hot water, the known magnitude, range, and remarkable uniformity of the thermal properties of most subsurface media allow this general statement. Predictions from the equilibrium and kinetic models may differ substantially in problems involving other dissociation methods such as pure depressurization, especially when the hydrate saturation is low and flows (and thermal advection) are high.

In this case, the total released volume at the end of the test period (including the sudden final release) is considered correct, and increased weight was given to the final data point in an effort to ensure that the history-matched curve passes by that point. The agreement with the field data is good. As expected, the curve for scenario B does not coincide with those from scenario A because the two correspond to different data sets.

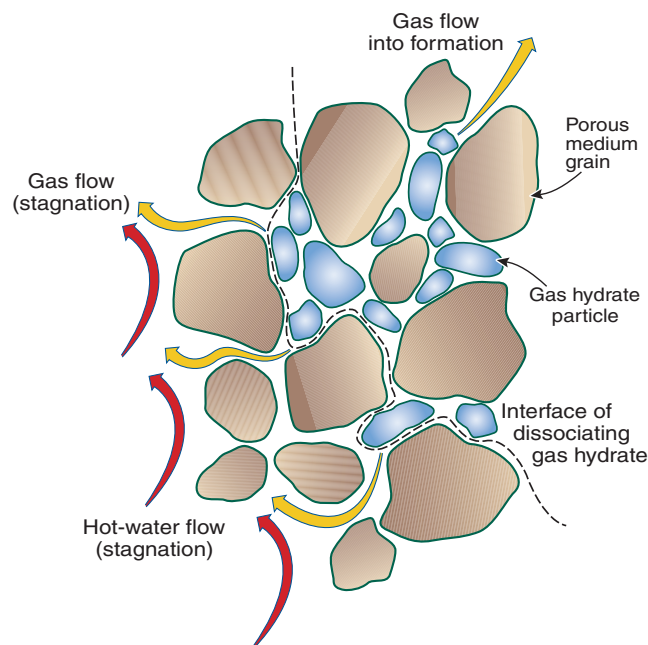


**Figure 16.** Schematic diagram of flow stagnation and gas escape into the formation because of the high-pressure ridge at the interface of the dissociating gas hydrate, JAPEx/JNOC/GSC et al. Mallik 5L-38 gas hydrate production research well. This is an oscillatory phenomenon that involves gas-pressure build-up and subsequent release.

### Parameter determination and general observations

For validation assuming fidelity to the trend of the production data and scenario B (equilibrium dissociation only), history matching required 46 iterations, and optimal results were obtained for the following parameters:

- base intrinsic permeability,  $k = 2 \times 10^{-13} \text{ m}^2$  (200 mD)
- gas hydrate specific heat,  $C_h = 1939 \text{ J/kg/}^\circ\text{C}$
- hydration number  $n_m = 6.3$
- rock thermal conductivity  $\kappa_R = 2.6 \text{ W/m/}^\circ\text{C}$
- gas hydrate thermal conductivity  $\kappa_h = 0.42 \text{ W/m/}^\circ\text{C}$

For validation assuming fidelity to the production data and scenario A, history matching for the case of equilibrium dissociation required 57 iterations, and optimal results were obtained for the following parameters:

- base (average) intrinsic permeability,  $k = 10^{-12} \text{ m}^2$  (1000 mD)
- gas hydrate specific heat,  $C_h = 2166 \text{ J/kg/}^\circ\text{C}$
- hydration number,  $n_m = 6.3$
- rock thermal conductivity,  $\kappa_R = 1.9 \text{ W/m/}^\circ\text{C}$
- gas hydrate thermal conductivity,  $\kappa_h = 0.42 \text{ W/m/}^\circ\text{C}$

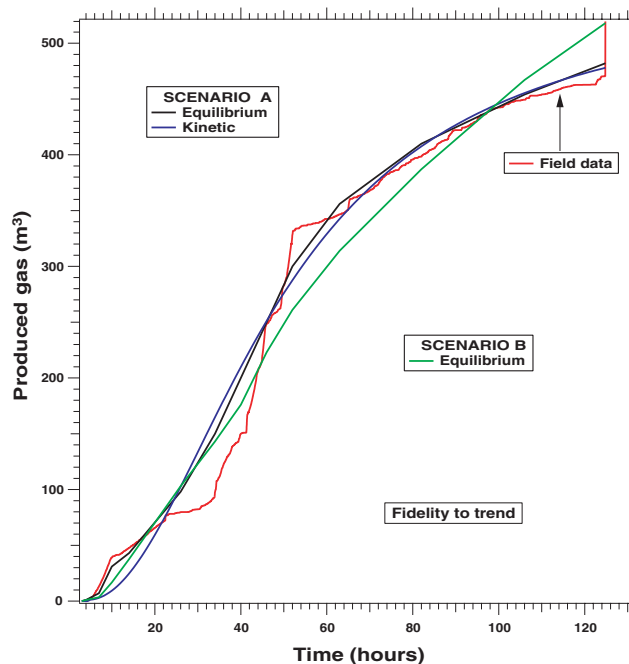


**Figure 17.** Comparison of measurements and numerical predictions (using calibrated parameters) in the validation attempt that assumes fidelity to the data trend (smoothed data are used), JAPEx/JNOC/GSC et al. Mallik 5L-38 gas hydrate production research well.

For validation assuming fidelity to the production data and scenario A, history matching for the case of kinetic dissociation required 76 iterations, and optimal results were obtained for the following parameters:

- base intrinsic permeability,  $k = 10^{-12} \text{ m}^2$  (1000 mD)
- gas hydrate specific heat,  $C_h = 1912 \text{ J/kg/}^\circ\text{C}$
- hydration number,  $n_m = 6.3$
- rock thermal conductivity,  $\kappa_R = 3.2 \text{ W/m/}^\circ\text{C}$
- gas hydrate thermal conductivity,  $\kappa_h = 0.47 \text{ W/m/}^\circ\text{C}$
- activation energy,  $\Delta E = 88.2 \text{ KJ/mol}$
- intrinsic dissociation rate constant,  $K_d^0 = 4.21 \times 10^4 \text{ mol/m}^2 \cdot \text{Pa} \cdot \text{s}$

In the case of parameters to which gas production exhibited limited sensitivity ( $n_m$  and  $\kappa_h$ ), their values were adjusted (through trial and error) to minimize the residuals after the remaining parameters had been determined from history matching. Spatial adjustments were necessary in the value of the base intrinsic permeability to improve the agreement with the field data. Note that smaller adjustments (e.g. changes in the porosity and gas hydrate saturation of individual grid blocks, adjustments in the fracture frequency of the fractured zone) were also made through trial and error in the process of history matching to obtain the best possible fits. In all the history-matching runs, the value of the area adjustment factor was maintained at  $f_A = 1$ .

There appears to be a relatively strong dependence on the type of dissociation (equilibrium versus kinetic) and  $\kappa_R$ , with kinetic dissociation associated with higher  $\kappa_R$  values. This is consistent with expectations, because higher thermal conductivity is needed to provide the same amount of heat to fuel dissociation in the slower kinetic process. The lower  $k$  deduced from history matching in scenario B (when assuming fidelity to trend) is compatible with the larger gas volume considered in this case, because the lower  $k$  increases gas flows to the well by significantly reducing the migration of the released gas deeper into the gas hydrate formation and away from the well.

The values of the history-matched gas hydrate properties and kinetic parameters compare favourably with the following previously published values:  $C_h = 2078 \text{ J/kg/}^\circ\text{C}$  (Sloan, 1998);  $\kappa_h = 0.42 \text{ W/m/}^\circ\text{C}$  (Sloan, 1998);  $5.75 \leq n_m \leq 7.2$  Sloan (1998);  $\Delta E = 78 \text{ KJ/mol}$  (Kim et al., 1987) and  $81 \text{ KJ/mol}$  (Clarke and Bishnoi, 2001);  $K_d^0 = 1.24 \times 10^5 \text{ mol/m}^2 \cdot \text{Pa} \cdot \text{s}$  (Kim et al., 1987); and  $K_d^0 = 3.6 \times 10^4 \text{ mol/m}^2 \cdot \text{Pa} \cdot \text{s}$  (Clarke and Bishnoi, 2001).

Thus, there is sufficient evidence to provide increased confidence in the model, based on

- the ability to accurately reproduce the field observations;
- the consistency between predictions of gas accumulation in the upper part of the formation and the geophysical-well-log data (Fig. 1; Anderson et al., 2005);

- the consistency between predictions of the extent and shape of the dissociation zone and the geophysical-well-log data (Fig. 15; Anderson et al., 2005); and
- the agreement between the values of the parameters determined from history matching and the published values.

Nevertheless, caution must be exercised before attempting to claim complete model validation, because different conceptual models are capable of providing almost equally good predictions using different parameter values. It is important to indicate that significant uncertainties remain (especially regarding the parameter estimation) because of knowledge gaps in the description of fundamental processes involved in gas hydrate dissociation (Moridis et al., 2004; Moridis, 2003, 2004a), the reliance on a single production data set, the very short duration of this field test, and the corresponding small total volume of produced gas (which were insufficient to ensure a data set free of the complex and dynamic phenomena that characterize the early stages of production in most gas wells). Additionally, the degrees of freedom corresponding to the relatively large number of components in the equations further complicate the issue by increasing the possibility of non-unique solutions. Studies and analyses of more data sets from longer term production tests are needed for complete model validation.

## PREDICTIONS OF LONG-TERM PRODUCTION

### *Parameters from data interpretation based on scenario A*

Figure 18 shows predictions of long-term gas production using different gas hydrate dissociation methods. For reference, the field measurements of the cumulative gas volume are also included. The parameters used in these studies were those determined from the data interpretation based on scenario A in the history-matching process discussed in the previous sections.

When the production period is extended to 3 years (26 300 hours), the cumulative volume released through thermal stimulation of the gas hydrate exhibits a very mild rate of increase after the first 100 hours, and reaches a total of about  $10^3 \text{ m}^3$  at the end of the simulation period (Fig. 18); equilibrium dissociation was assumed in this case. This result indicates the inefficiency of thermal stimulation by hot-fluid circulation as a production method, and was expected because of the progressively smaller amount of heat available for dissociation. As time advances, increasing amounts of heat are wasted because of heat fluxes through expanding areas of the top and bottom flow boundaries. Additionally, the very large thermal inertia of the porous-media grains in the expanding dissociated zone, and the need to maintain a minimum temperature at the dissociation front, require ever increasing amounts of heat, reducing correspondingly the heat available for dissociation.

The evolution of the released volume in the case of gas production through depressurization (through gas lift to 25% of the hydrostatic pressure) shows a slower initial release

rate, which later overtakes that for thermal stimulation before reaching a plateau of a little over  $10^3 \text{ m}^3$  after about  $10^3$  hours. The slower initial dissociation is a result of the kinetic dissociation used in this study (necessary because depressurization is a much milder process than thermal stimulation), and is followed by a period of rapid production as the partially dissociated (and increasingly permeable) zone increases, along with the ease of dissociation. Dissociation stops almost completely at  $10^3$  hours, however, because the strongly endothermic nature of the gas hydrate dissociation reaction makes gas release progressively more difficult and eventually leads to freezing of the water. At that point, dissociation is severely reduced, while hydrate formation in the vicinity of the wellbore reduces the permeability and inhibits flow to the wellbore.

The cumulative gas production is significantly larger when thermal stimulation and depressurization (through a gas lift to 25% of the hydrostatic pressure) are combined. In this case, no production plateau is reached, gas is continuously produced at substantial rates, and the cumulative gas production at  $t = 3$  years is about  $7 \times 10^4 \text{ m}^3$  (i.e. orders of magnitude larger than that for either thermal stimulation or depressurization alone). Thus, the combined effect of the two dissociation methods is multiplicative rather than additive. Although gas production is much larger than in the other two cases, it is still quite low in absolute terms, a level attributed to the very conservative estimates of the parameters used in the simulations.

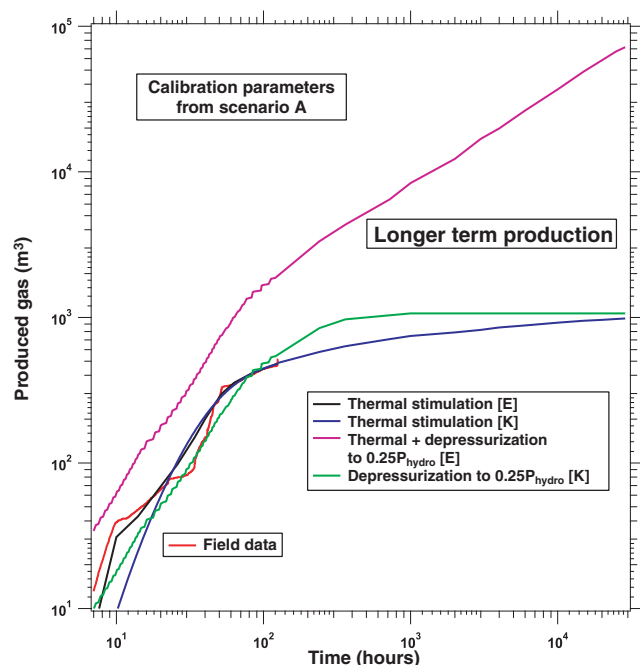


**Figure 18.** Predictions of long-term production for the JAPEX/JNOC/GSC et al. Mallik 5L-38 gas hydrate production research well using the calibrated parameters from the data interpretation based on scenario A. Abbreviations: [E], equilibrium dissociation; [K], kinetic dissociation.

### Parameters from data interpretation based on scenario B

When parameters from the data interpretation from scenario B are used, the cumulative gas production increases by orders of magnitude (Fig. 19). Simple depressurization was not considered in this study because of the problem of cessation of dissociation discussed in the previous section. Although thermal stimulation results in much higher volumes (about  $3 \times 10^4 \text{ m}^3$  at  $t = 3$  years) than in scenario A, these are still very low when compared to gas production from conventional sources. A significant increase in cumulative gas production is also observed in the case of combined thermal stimulation and depressurization, in which about  $8.5 \times 10^5 \text{ m}^3$  are released at the end of the three-year production period.

### ALTERNATIVE PRODUCTION SYSTEM

Although the combination of thermal stimulation and depressurization is the most promising among the dissociation methods studied thus far, the single vertical well configuration used in these studies suffers from a significant shortcoming. As the dissociated zone expands into the formation, depressurization tends to increasingly short-circuit the effect of thermal stimulation, because the pressure regime does not allow significant penetration of the hot water into the formation. Thus, the advective component of heat transport becomes progressively

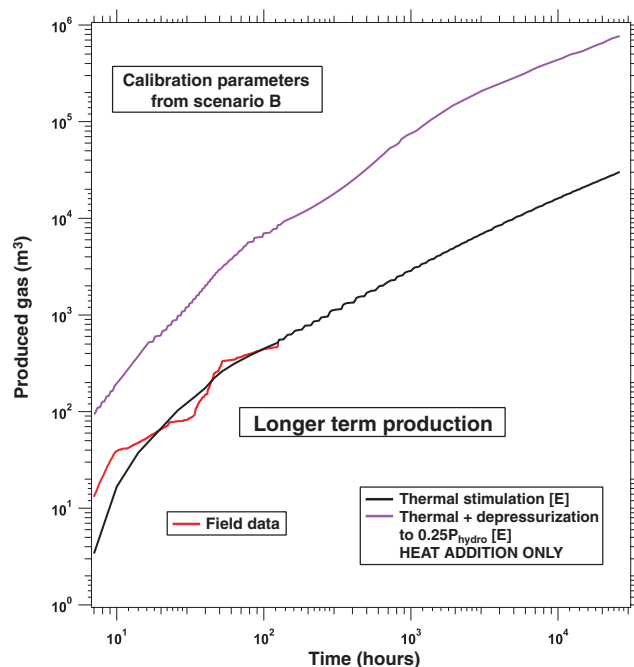


**Figure 19.** Predictions of long-term production for the JAPEX/JNOC/GSC et al. Mallik 5L-38 gas hydrate production research well using the calibrated parameters based on the scenario B. Abbreviation: [E], equilibrium dissociation.

smaller because of preferential flow toward the well (caused by the lower pressure), coupled with the increased pressure resulting from the gas release. Consequently, the slow and inefficient process of conduction emerges as the main method of heat transport at later times, limiting the overall production potential.

To alleviate this problem, the alternative well configuration of Figure 20 is proposed. Instead of a vertical well used for both thermal stimulation and depressurization, the well has both a vertical component and a long horizontal component running along the centre plane of the gas hydrate accumulation. Gas production proceeds in two phases. During the first phase, the vertical component of the well is used for both thermal stimulation and depressurization, and serves to produce a permeable pathway to the gas collection system. In the second phase of production (after the gas hydrate has dissociated to a sufficiently large radius), the vertical component of the well is used exclusively for depressurization and gas collection, while the long horizontal component of the well is used for thermal stimulation.

The horizontal well component is not perforated and is used to provide only heat to the gas-hydrate-bearing formation (e.g. through electrical heating). By avoiding the injection of fluids (such as hot water), a far more favourable relative permeability environment is created in the dissociating system as the free gas zone keeps expanding in the course of production.

To ensure proper communication with (and a fast permeability pathway to) the dissociated zone that envelops the vertical component of the well, a gravel pack completion is needed around the horizontal well component. By keeping the vertical component at a low pressure, providing sufficient heat to fuel gas hydrate dissociation, and keeping the main locations of depressurization and thermal stimulation physically separated by a substantial distance, the released gas moves easily toward the well without any stagnation at the dissociation front.

Heating does not occur continuously along the entire length of the horizontal well component, but proceeds in successive segments as a travelling heating system. Thus, heating ceases in the well segment that corresponds to a largely dissociated formation, and begins in the next segment of undisturbed gas hydrate. The segment length, and the rate and duration of heat addition, depend on the thickness of the gas hydrate interval, with heating ceasing (and beginning in the next well segment) when the thermal front is about to reach the impermeable boundaries (see the depiction on the  $yz$  plane in Fig. 20). In the case of long-term production from the Mallik 5L-38 well and the 906 to 930 m gas hydrate interval, 100 m long segments of the horizontal well were used for the simulation. In each of the sequential segments, heat was added continuously for 6 months at a rate of 0.6 W/m of length (determined through preliminary scoping calculations).

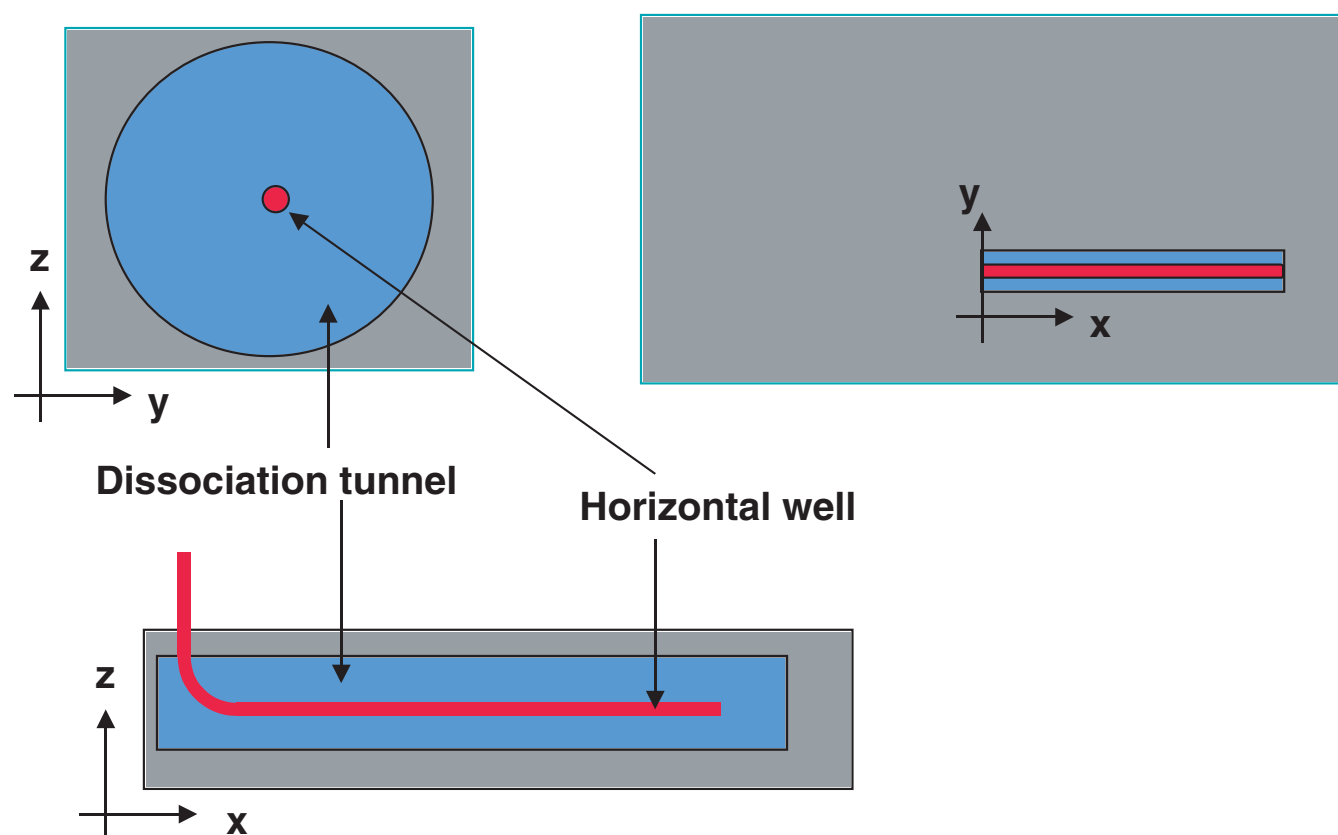


**Figure 20.** Configuration of a well system for increased gas production from Class 3 gas hydrate accumulations such as that at the JAPEx/JNOC/GSC et al. Mallik 5L-38 gas hydrate production research well.

This well configuration leads to the formation of a dissociation tunnel (Fig. 20), in which the dissociation front moves continuously away from the vertical main stem as successive horizontal segments are heated. The physical separation between the low-pressure gas-collection point in the vertical component of the well and the dissociation interface creates a favourable permeability regime and facilitates flow to the well. Note that more than one horizontal well can originate from a single vertical stem (a rather well developed technology), thus significantly enhancing the production potential.

Figure 21 shows the cumulative gas production from such a well configuration when the parameters from the scenario B data interpretation are used. Equilibrium dissociation was assumed in these simulations. Because of symmetry, only half of the three-dimensional (3-D) domain corresponding to the horizontal well (installed on the centre plane of the accumulation) was simulated, using a grid composed of  $40 \times 40 \times 40 = 64\,000$  grid blocks in (x, y, z). Because the vertical component of the well is used for both depressurization (to 25% of the hydrostatic pressure) and thermal stimulation, the produced volume was adjusted to coincide with that in Figure 18 during the first phase of production (the adjustment is necessary to account for differences caused by the coarser 3-D grid). The conditions at the end of the first phase were used as the initial conditions for the second phase. In the second phase of production, the use of a single dissociation tunnel increased cumulative production from about  $8.5 \times 10^5 \text{ m}^3$  to about  $1.2 \times 10^7 \text{ m}^3$  at the end of the three-year production period. Total gas production can increase linearly for multiple dissociation tunnels operating concurrently.

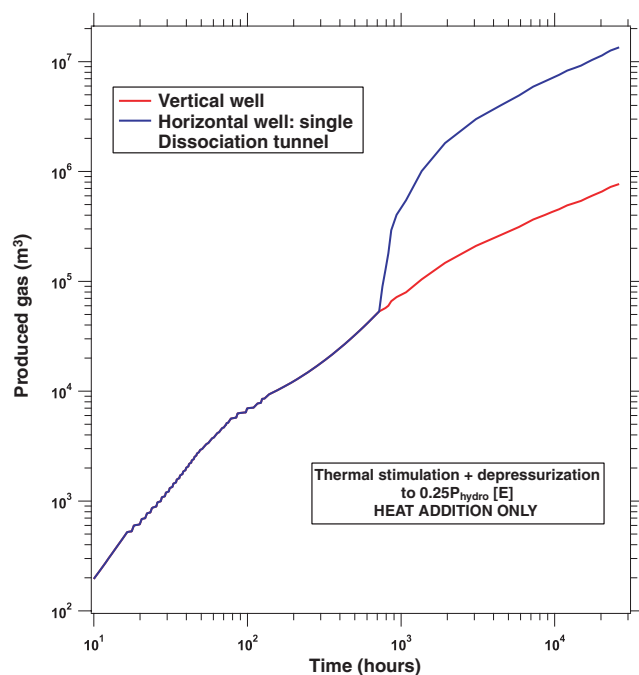


**Figure 21.** Long-term gas production from the Class 3 gas hydrate deposit at the Mallik site using the well configuration depicted in Figure 19. Abbreviation: [E], equilibrium dissociation.

## CONCLUSIONS

The following conclusions resulted from this study:

- By using inverse modelling (history matching), it is possible to numerically reproduce (match) the gas production observed in the course of the thermal test at the JAPEx/JNOC/GSC et al. Mallik 5L-38 gas hydrate production research well, through development of plausible dissociation scenarios.
- The calibrated parameters compare favourably with literature values, and the simulated gas and gas hydrate saturation distributions at the end of the thermal test are consistent with geophysical-well-log data. These agreements tend to support the claim of model validation.
- Caution should be exercised in the interpretation of the data (because of the limited data-gathering period) and the exploration of long-term production scenarios.
- For Class 3 gas hydrate deposits such as the one at the Mallik 5L-38 research well site, pure thermal stimulation or depressurization in conventional well configurations lead to small total production. Combination of depressurization and thermal stimulation appears to be the most promising production strategy.
- Innovative approaches will be required for production from Class 3 hydrate deposits to become commercially viable.

## ACKNOWLEDGMENTS

This study was supported by the Assistant Secretary for Fossil Energy, Office of Natural Gas and Petroleum Technology, under United States Department of Energy Contract No. DE-AC03-76SF00098. The authors gratefully acknowledge the international partnership that undertook the Mallik 2002 Gas Hydrate Production Research Well Program: Geological Survey of Canada (GSC), Japan National Oil Corporation (JNOC), GeoForschungsZentrum Potsdam (GFZ), United States Geological Survey (USGS), United States Department of Energy (USDOE), India Ministry of Petroleum and Natural Gas (MOPNG), and the BP-ChevronTexaco-Burlington joint venture parties. The Mallik 2002 project also received critical financial support from the International Continental Scientific Drilling Program (ICDP). The authors are indebted to Karsten Pruess, John Apps, and Dan Hawkes of Lawrence Berkeley National Laboratory for their insightful review comments.

## REFERENCES

- Anderson, B., Dubourg, I., Collett, T.S., and Lewis, R.**  
2005: Modelling the response of the cased hole formation resistivity tool in order to determine the depth of gas hydrate dissociation during the thermal test in the JAPEX/JNOC/GSC et al. Mallik 5L-28 gas hydrate production research well; *in* Scientific Results from the Mallik 2002 Gas Hydrate Production Research Well Program, Mackenzie Delta, Northwest Territories, Canada, (ed.) S.R. Dallimore and T.S. Collett; Geological Survey of Canada, Bulletin 585.
- Bear, J.**  
1972: *Dynamics of Fluids in Porous Media*; American Elsevier Inc., New York, New York, 764 p.
- Bejan, A.**  
1984: *Convection Heat Transfer*; John Wiley and Sons, New York, New York, 454 p.
- Bily, C. and Dick, J.W.L.**  
1974: Naturally occurring gas hydrates in the Mackenzie Delta, Northwest Territories, Canada, (ed.) S.R. Dallimore, T. Uchida, and T.S. Collett; Geological Survey of Canada, Bulletin 544, p. 340–352.
- Clarke, M. and Bishnoi, P.R.**  
2001: Determination of activation energy and intrinsic rate constant of methane gas hydrate decomposition; *Canadian Journal of Chemical Engineering*, v. 79, no. 1, p. 143–147.
- Collett, T.S., Lewis, R.E., Dallimore, S.R., Lee, M.W., Mroz, T.H., and Uchida, T.**  
1999: Detailed evaluation of gas hydrate reservoir properties using JAPEX/JNOC/GSC Mallik 2L-38 gas hydrate research well downhole well-log displays; *in* Scientific Results from JAPEX/JNOC/GSC Mallik 2L-38 Gas Hydrate Research Well, Mackenzie Delta, Northwest Territories, Canada, (ed.) S.R. Dallimore, T. Uchida, and T.S. Collett; Geological Survey of Canada, Bulletin 544, p. 295–311.
- Dallimore, S.R. and Collett, T.S.**  
1999: Regional hydrate occurrences, permafrost conditions, and Cenozoic geology, Mackenzie Delta area; *in* Scientific Results from JAPEX/JNOC/GSC Mallik 2L-38 Gas Hydrate Research Well, Mackenzie Delta, Northwest Territories, Canada, (ed.) S.R. Dallimore, T. Uchida, and T.S. Collett; Geological Survey of Canada, Bulletin 544, p. 31–43.
- Dallimore, S.R., Collett, T.S., and Uchida, T.**  
1999: Overview of science program, JAPEX/JNOC/GSC Mallik 2L-38 gas hydrate research well; *in* Scientific Results from JAPEX/JNOC/GSC Mallik 2L-38 Gas Hydrate Research Well, Mackenzie Delta, Northwest Territories, Canada, (ed.) S.R. Dallimore, T. Uchida, and T.S. Collett; Geological Survey of Canada, Bulletin 544, p. 11–17.
- Dallimore, S.R., Collett, T.S., Uchida, T., and Weber, M.**  
2005: Overview of the science program for the Mallik 2002 Gas Hydrate Production Research Well Program; *in* Scientific Results from the Mallik 2002 Gas Hydrate Production Research Well Program, Mackenzie Delta, Northwest Territories, Canada, (ed.) S.R. Dallimore and T.S. Collett; Geological Survey of Canada, Bulletin 585.
- de Marsily, G.**  
1986: *Quantitative Hydrogeology*; Academic Press, San Diego, California, 440 p.
- Frost, H.J.**  
2001: Mechanisms of crack nucleation in ice; *Engineering Fracture Mechanics*, v. 68, p. 1823–1837.
- Hancock, S.H., Collett, T.S., Dallimore, S.R., Satoh, T., Inoue, T., Huenges, E., Henningses, J., and Weatherill, B.**  
2005: Overview of thermal-stimulation production-test results for the JAPEX/JNOC/GSC et al. Mallik 5L-38 gas hydrate production research well; *in* Scientific Results from the Mallik 2002 Gas Hydrate Production Research Well Program, Mackenzie Delta, Northwest Territories, Canada, (ed.) S.R. Dallimore and T.S. Collett; Geological Survey of Canada, Bulletin 585.
- Henningses, J., Schrötter, J., Erbas, K., and Huenges, E.**  
2005: Temperature field of the Mallik gas hydrate occurrence — implications on phase changes and thermal properties; *in* Scientific Results from the Mallik 2002 Gas Hydrate Production Research Well Program, Mackenzie Delta, Northwest Territories, Canada, (ed.) S.R. Dallimore and T.S. Collett; Geological Survey of Canada, Bulletin 585.
- Jenner, K.A., Dallimore, S.R., Clark, I.D., Paré, D., and Medioli, B.E.**  
1999: Sedimentology of gas hydrate host strata from the JAPEX/JNOC/GSC Mallik 2L-38 gas hydrate research well; *in* Scientific Results from JAPEX/JNOC/GSC Mallik 2L-38 Gas Hydrate Research Well, Mackenzie Delta, Northwest Territories, Canada, (ed.) S.R. Dallimore, T. Uchida, and T.S. Collett; Geological Survey of Canada, Bulletin 544, p. 57–68.
- Kamath, V.A.**  
1984: Study of heat transfer characteristics during dissociation of gas hydrates in porous media; Ph.D. thesis, University of Pittsburgh, University Microfilms No. 8417404, Ann Arbor, Michigan.
- Kim, H.C., Bishnoi, P.R., Heidemann, R.A., and Rizvi, S.S.H.**  
1987: Kinetics of methane hydrate decomposition; *Chemical Engineering Science*, v. 42, no. 7, p. 1645–1653.
- Leverett, M.C.**  
1941: Capillary behavior in porous solids; *Transactions of the American Society of Petroleum Engineers of the American Institute of Mining Engineers*, v. 142, p. 152–169.
- Lewis, R. and Collett, T.S.**  
2005: JAPEX/JNOC/GSC et al. Mallik 5L-38 gas hydrate production research well downhole well-log and core montages; *in* Scientific Results from the Mallik 2002 Gas Hydrate Production Research Well Program, Mackenzie Delta, Northwest Territories, Canada, (ed.) S.R. Dallimore and T.S. Collett; Geological Survey of Canada, Bulletin 585.
- Lorenson, T.D., Whiticar, M.J., Collett, T.S., Dallimore, S.R., and Dougherty, J.A.**  
2005: Complete gas composition and isotopic geochemistry from the JAPEX/JNOC/GSC et al. Mallik 5L-38 gas hydrate production research well: cuttings, core, gas hydrate, and production testing results; *in* Scientific Results from the Mallik 2002 Gas Hydrate Production Research Well Program, Mackenzie Delta, Northwest Territories, Canada, (ed.) S.R. Dallimore and T.S. Collett; Geological Survey of Canada, Bulletin 585.
- Miyairi, M., Akihisa, K., Uchida, T., Collett, T.S., and Dallimore, S.R.**  
1999: Well-log interpretation of gas-hydrate-bearing formations in the JAPEX/JNOC/GSC Mallik 2L-38 gas hydrate research well; *in* Scientific Results from JAPEX/JNOC/GSC Mallik 2L-38 Gas Hydrate Research Well, Mackenzie Delta, Northwest Territories, Canada, (ed.) S.R. Dallimore, T. Uchida, and T.S. Collett; Geological Survey of Canada, Bulletin 544, p. 281–293.
- Moridis, G.J.**  
2003: Numerical studies of gas production from methane hydrates; *Society of Petroleum Engineers Journal*, v. 32, no. 8, p. 359–370.  
2004a: Numerical studies of gas production from methane hydrates; *Society of Petroleum Engineers Reservoir Evaluation and Engineering*, v. 27, no. 3, p. 175–183.  
2004b: TOUGH-Fx/HYDRATE v1.0: a code for the simulation of system behavior in hydrate-bearing geologic media; Lawrence Berkeley National Laboratory, Berkeley, California, Report LBNL-77328.
- Moridis, G.J. and Collett, T.S.**  
2003: Strategies for gas production from hydrate accumulations under various geologic conditions; Lawrence Berkeley National Laboratory, Berkeley, California, Report LBNL-53568.
- Moridis, G.J., Collett, T.S., Dallimore, S.R., Satoh, T., Hancock, S., and Weatherill, B.**  
2004: Numerical studies of gas production from several methane hydrate zones at the Mallik site, Mackenzie Delta, Canada; *Journal of Petroleum Science and Engineering*, v. 43, p. 219–239 (also Lawrence Berkeley National Laboratory, Berkeley, California, Report LBNL-50257, 2002).
- Mualem, Y.**  
1976: A new model for predicting the hydraulic conductivity of unsaturated porous media; *Water Resources Research*, v. 23, no. 4, p. 618–624.
- Parker, J.C., Lenhard, R.J., and Koppusamy, T.**  
1987: A parametric model for constitutive properties governing multiphase flow in porous media; *Water Resources Research*, v. 12, p. 513–522.
- Perkins, T.K. and Gonzalez, J.A.**  
1985: A parametric model for constitutive properties governing multiphase flow in porous media; *Society of Petroleum Engineers Journal*, February, p. 78–88.
- Pruess, K.**  
1991: TOUGH2 – a general-purpose numerical simulator for multiphase fluid and heat flow; Lawrence Berkeley Laboratory, Berkeley, California, Report LBNL-29400.

**Pruess, K., Oldenburg, C., and Moridis, G.J.**

1999: TOUGH2 User's Guide – Version 2.0; Lawrence Berkeley National Laboratory, Berkeley, California, Report LBNL-43134.

**Satoh T., Dallimore, S.R., Collett, T.S., Inoue, T., Hancock, S.H., Moridis, G., and Weatherill, B.**

2005: Production-test planning for the JAPEX/JNOC/GSC et al. Mallik 5L-38 gas hydrate production research well; *in* Scientific Results from the Mallik 2002 Gas Hydrate Production Research Well Program, Mackenzie Delta, Northwest Territories, Canada, (ed.) S.R. Dallimore and T.S. Collett; Geological Survey of Canada, Bulletin 585.

**Sloan, E.D. (ed.)**

1998: Clathrate Hydrates of Natural Gases; Marcel Dekker, Inc., New York, New York, 705 p. (second edition).

**Stone, H.L.**

1970: Probability model for estimating three-phase relative permeability; Transactions of the Society of Petroleum Engineers of the American Institute of Mining Engineers, v. 249, p. 214–218.

**Takahashi, H., Fercho, E., and Dallimore, S.R.**

2005: Drilling and operations overview of the Mallik 2002 Production Research Well Program; *in* Scientific Results from the Mallik 2002 Gas Hydrate Production Research Well Program, Mackenzie Delta, Northwest Territories, Canada, (ed.) S.R. Dallimore and T.S. Collett; Geological Survey of Canada, Bulletin 585.

**Thomas, L.K., Hellums, T.S., and Reheis, G.M.**

1972: A nonlinear automatic history matching technique for reservoir simulation models; SPE paper 3475 *in* SPE Reprint Series, No. 11: Numerical Simulation; Society of Petroleum Engineers of the American Institute of Mining Engineers, 1973 edition, p. 106–112.

**Tulk, C.A., Ratcliffe, C.I., and Ripmeester, J.A.**

1999: Chemical and physical analysis of natural gas hydrate from the JAPEX/JNOC/GSC Mallik 2L-38 gas hydrate research well; *in* Scientific Results from JAPEX/JNOC/GSC Mallik 2L-38 Gas Hydrate Research Well, Mackenzie Delta, Northwest Territories, Canada, (ed.) S.R. Dallimore, T. Uchida, and T.S. Collett; Geological Survey of Canada, Bulletin 544, p. 251–262.

**Warren, J.E. and Root, P.J.**

1963: The behavior of naturally fractured reservoirs; Society of Petroleum Engineers Journal, Transactions of the American Institute of Mining Engineers, v. 228, p. 245–255.

**Wiersberg, T., Erzinger, J., Zimmer, M., Schicks, J., and Dahms, E.**

2005: Real-time gas analysis at the JAPEX/JNOC/GSC et al. Mallik 5L-28 gas hydrate production research well; *in* Scientific Results from the Mallik 2002 Gas Hydrate Production Research Well Program, Mackenzie Delta, Northwest Territories, Canada, (ed.) S.R. Dallimore and T.S. Collett; Geological Survey of Canada, Bulletin 585.

**Wright, J.F., Dallimore, S.R., and Nixon, F.M.**

1999: Influences of grain size and salinity on pressure-temperature thresholds for methane hydrate stability in JAPEX/JNOC/GSC Mallik 2L-38 gas hydrate research-well sediments; *in* Scientific Results from JAPEX/JNOC/GSC Mallik 2L-38 Gas Hydrate Research Well, Mackenzie Delta, Northwest Territories, Canada, (ed.) S.R. Dallimore, T. Uchida, and T.S. Collett; Geological Survey of Canada, Bulletin 544, p. 229–239.

**Wright, J.F., Nixon, F.M., Dallimore, S.R., Henningses, J., and Côté, M.M.**

2005: Thermal conductivity of sediments within the gas-hydrate-bearing interval at the JAPEX/JNOC/GSC et al. Mallik 5L-38 gas hydrate production research well; *in* Scientific Results from the Mallik 2002 Gas Hydrate Production Research Well Program, Mackenzie Delta, Northwest Territories, Canada, (ed.) S.R. Dallimore and T.S. Collett; Geological Survey of Canada, Bulletin 585.